

Validation of SAGE III/ISS Solar Ozone Data with Correlative Satellite and Ground Based Measurements

H. J. Ray Wang¹, Robert Damadeo², David E. Flittner², Natalya A Kramarova³, Ghassan Taha⁴, Sean M. Davis⁵, Anne M. Thompson⁶, Susan E Strahan⁴, Yuhang Wang¹, Lucien Froidevaux⁷, Douglas A. Degenstein⁸, Adam E. Edward Bourassa⁸, Wolfgang Steinbrecht⁹, Kaley A. Walker¹⁰, Richard Querel¹¹, Thierry Leblanc¹², Sophie Godin-Beekmann¹³, Dale F. Hurst¹⁴, and Emrys Hall¹⁵

¹Georgia Institute of Technology

²NASA Langley Research Center

³Science Systems and Applications, Inc.,

⁴Universities Space Research Association

⁵NOAA ESRL

⁶NASA-GODDARD

⁷JPL/California Institute of Technology, California, USA

⁸University of Saskatchewan

⁹Deutscher Wetterdienst

¹⁰University of Toronto

¹¹National Institute of Water & Atmospheric Research (NIWA)

¹²California Institute of Technology

¹³LATMOS, CNRS, UVSQ, UPMC

¹⁴NOAA Earth System Research Laboratory

¹⁵NOAA Earth Systems Research Laboratory

November 22, 2022

Abstract

The Stratospheric Aerosol and Gas Experiment III on the International Space Station (SAGE III/ISS) was launched on February 19, 2017 and began routine operation in June 2017. The first two years of SAGE III/ISS (v5.1) solar ozone data were evaluated by using correlative satellite and ground-based measurements. Among the three (MES, AO3, and MLR) SAGE III/ISS solar ozone products, AO3 ozone shows the best accuracy and precision, with mean biases less than 5% for altitudes ~15–55 km in the mid-latitudes and ~20–55 km in the tropics. In the lower stratosphere and upper troposphere, AO3 ozone shows high biases that increase with decreasing altitudes and reach ~10% near the tropopause. Preliminary studies indicate that those high biases primarily result from the contributions of the oxygen dimer (O₂) not being appropriately removed within the ozone channel. The precision of AO3 ozone is estimated to be ~3% for altitudes between 20 and 40 km. It degrades to ~10–15% in the lower mesosphere (~55 km), and ~20–30% near the tropopause. There could be an altitude registration error of ~100 meter in the SAGE III/ISS auxiliary temperature and pressure profiles. This, however, does not affect retrieved ozone profiles in native number density on geometric altitude coordinates. In the upper stratosphere and lower mesosphere (~40–55 km) the SAGE III/ISS (and SAGE II) sunset ozone values are systematically higher than sunrise data by ~5–8% which are almost twice larger than what observed by other satellites or model predictions. This feature needs further study.

Validation of SAGE III/ISS Solar Ozone Data with Correlative Satellite and Ground Based Measurements

H.J. Ray Wang¹, Robert Damadeo², David Flittner², Natalya Kramarova³, Ghassan Taha⁴, Sean Davis⁵, Anne M. Thompson³, Susan Strahan⁴, Yuhang Wang¹, Lucien Froidevaux⁶, Doug Degenstein⁷, Adam Bourassa⁷, Wolfgang Steinbrecht⁸, Kaley A. Walker⁹, Richard Querel¹⁰, Thierry Leblanc¹¹, Sophie Godin-Beekmann¹², Dale Hurst^{13,14}, Emrys Hall^{13,14}

¹School of Earth and Atmospheric Sciences, Georgia Institute of Technology, Atlanta, GA, USA

²NASA Langley Research Center, Hampton, VA, USA

³NASA Goddard Space Flight Center, Greenbelt, MD, USA

⁴Universities Space Research Association, NASA/Code 614, Greenbelt, MD, USA

⁵NOAA Earth System Research Laboratory Chemical Sciences Division, Boulder, CO, USA

⁶Jet Propulsion Laboratory, California Institute of Technology, Pasadena, CA, USA

⁷Institute of Space and Atmospheric Studies, University of Saskatchewan, Saskatoon, Saskatchewan, Canada

⁸Deutscher Wetterdienst, Hohenpeissenberg, Germany

⁹Department of Physics, University of Toronto, Toronto, Ontario, Canada

¹⁰National Institute of Water & Atmospheric Research (NIWA), Lauder, New Zealand

¹¹Jet Propulsion Laboratory, California Institute of Technology, Wrightwood, CA 92397, USA

¹²LATMOS-ISPL, Université Paris 6 Pierre-et-Marie-Curie, Paris, France

¹³Cooperative Institute for Research in Environmental Sciences, University of Colorado, Boulder, CO, USA

¹⁴NOAA Earth System Research Laboratory Global Monitoring Division, Boulder, CO, USA

Corresponding author: H.J. Ray Wang (raywang@eas.gatech.edu).

Key Points:

- Among the three SAGE III/ISS solar occultation retrievals, AO3 ozone product shows the best accuracy and precision.
- The mean biases of AO3 ozone are less than 5% for ~15–55 km in the mid-latitudes and ~20–55 km in the tropics. It increases to ~10% near the tropopause.
- The precision of AO3 ozone is ~3% for altitudes 20–40 km. It degrades to ~10–15% in the lower mesosphere (~55 km), and ~20–30% near the tropopause.

34 **Abstract**

35 The Stratospheric Aerosol and Gas Experiment III on the International Space Station (SAGE
36 III/ISS) was launched on February 19, 2017 and began routine operation in June 2017. The first
37 two years of SAGE III/ISS (v5.1) solar ozone data were evaluated by using correlative satellite
38 and ground-based measurements. Among the three (MES, AO3, and MLR) SAGE III/ISS solar
39 ozone products, AO3 ozone shows the best accuracy and precision, with mean biases less than
40 5% for altitudes ~15–55 km in the mid-latitudes and ~20–55 km in the tropics. In the lower
41 stratosphere and upper troposphere, AO3 ozone shows high biases that increase with decreasing
42 altitudes and reach ~10% near the tropopause. Preliminary studies indicate that those high biases
43 primarily result from the contributions of the oxygen dimer (O₄) not being appropriately
44 removed within the ozone channel. The precision of AO3 ozone is estimated to be ~3% for
45 altitudes between 20 and 40 km. It degrades to ~10–15% in the lower mesosphere (~55 km), and
46 ~20–30% near the tropopause. There could be an altitude registration error of ~100 meter in the
47 SAGE III/ISS auxiliary temperature and pressure profiles. This, however, does not affect
48 retrieved ozone profiles in native number density on geometric altitude coordinates. In the upper
49 stratosphere and lower mesosphere (~40–55 km) the SAGE III/ISS (and SAGE II) sunset ozone
50 values are systematically higher than sunrise data by ~5–8% which are almost twice larger than
51 what observed by other satellites or model predictions. This feature needs further study.

52 **1 Introduction**

53 The Stratospheric Aerosol and Gas Experiment III on the International Space Station
54 (SAGE III/ISS) is the second instrument from the SAGE III project. It was launched on a
55 SpaceX Falcon 9/Dragon spacecraft on February 19, 2017 and began routine operation in June
56 2017. Similar to its predecessors, SAGE I (1979–1981), SAGE II (1984–2005), and SAGE
57 III/M3M (2001–2006), SAGE III/ISS uses the solar occultation technique to retrieve vertical
58 profiles of ozone (O₃), water vapor (H₂O), nitrogen dioxide (NO₂), and aerosol extinctions at
59 multiple wavelengths (e.g., Mauldin et al., 1985; McCormick et al., 1993; Wang et al., 2006;
60 Thomason et al., 2010). In addition, SAGE III can utilize the multi-spectral measurement of the
61 oxygen A-band (758–771 nm) to derive vertical profiles of temperature and pressure (Pitts and
62 Thomason, 2003). The SAGE series of observations has provided valuable data for
63 understanding global ozone trends (SPARC/IO3C/GAW, 2019; WMO, 2018) and the impact of
64 volcanoes and human activities on stratospheric aerosol (SPARC, 2006).

65 SAGE III/ISS can also observe the atmosphere at night by using the lunar occultation
66 technique. Lunar occultation is achieved by rotating the solar attenuator out of the optical path
67 and using a fully programmable Charged Couple Device (CCD) that enables selection of
68 different spectral channels and integration times. The lunar observations can provide vertical
69 profiles of ozone (O₃), nitrogen dioxide (NO₂), nitrogen trioxide (NO₃), and chlorine dioxide
70 (OCIO). A separate algorithm (e.g., Rault, 2005; Rault and Loughman, 2013) is being developed
71 to retrieve trace gases from limb scattering measurements, which are still research products and
72 not yet available to the public.

73 Unlike the first SAGE III instrument on the Meteor 3M spacecraft (SAGE III/M3M),
74 which was in a sun synchronous orbit providing observations in the northern hemisphere at mid
75 to high latitudes (~45°–80°N), and in the southern hemisphere at mid-latitudes (~35°–60°S),
76 SAGE III/ISS is in a mid-inclination orbit (51.6°). The solar observations can provide near
77 global (~70°S–70°N) measurements on a monthly basis with coverage similar to that of the

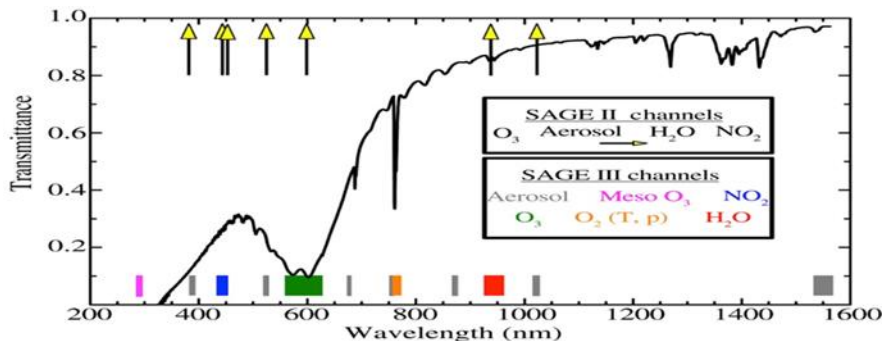
78 SAGE II measurements. There is, however, some loss of measurements due to the obscuration of
 79 the Sun by the ISS and limitations to operations due to spacecraft visits to ISS. The sampling
 80 coverage of SAGE III/ISS solar observations can be augmented by lunar measurements, which
 81 occur at locations and times not covered by solar observations.

82 In this paper, we evaluate the quality of SAGE III/ISS version 5.1 solar ozone data by
 83 comparisons with other independent measurements from satellites as well as ozonesondes and
 84 lidar. Section 2 describes the SAGE III retrieval algorithm, solar ozone products and some
 85 known anomalies in the current algorithm. The correlative satellite and ground-based datasets are
 86 described in section 3. Section 4 describes the coincident criteria and validation methodology.
 87 The comparison results are shown in section 5 and followed by the conclusions in section 6.

88 2 SAGE III/ISS solar ozone data

89 2.1 Instrument and retrieval overview

90 The SAGE III instruments makes solar occultation measurements by scanning a
 91 relatively small field-of-view (0.5 arcminutes in the vertical and 5.0 arcminutes in the horizontal)
 92 vertically across the face of the Sun and focusing the light into a simple grating spectrometer.
 93 The spectrometer uses a CCD array with 809 spectral columns with resolutions of $\sim 1\text{--}2$ nm that
 94 provide nearly continuous spectral coverage between ~ 280 and ~ 1035 nm as well as a single
 95 photodiode covering $1542 \text{ nm} \pm 15 \text{ nm}$. These 809 CCD pixels are then subsampled (i.e., read
 96 out individually or co-added or averaged with other pixels) into a number of “pixel groups” that
 97 change for different modes of operation. For solar occultation, there are 86 of these pixel groups
 98 (87 including the photodiode) that fall into 12 different channels illustrated in Fig. 1. For
 99 comparison, the central wavelength of the seven channels used by SAGE II are also shown in
 100 Figure 1.



101
 102 **Figure 1:** Sample wavelength dependence of atmospheric transmission in the lower stratosphere
 103 with locations of the different spectral channels used by the SAGE II (yellow arrows) and SAGE
 104 III/ISS instruments (colored boxes). The twelve SAGE III/ISS channels are color-coded by
 105 species of interest and are numbered from smallest to largest wavelength.

106 The current retrieval algorithm for SAGE III/ISS is version 5.1, which is essentially the
 107 same as that used for SAGE III/M3M. A complete description of the SAGE III retrieval
 108 algorithm is available in the SAGE III Algorithm Theoretical Basis Document: Solar and Lunar
 109 Algorithm (SAGE III ATBD, 2002). The algorithm consists of two main parts, the transmission
 110 algorithm and the species inversion algorithm. The transmission algorithm involves taking the
 111 raw uncalibrated radiance counts from the CCD (and photodiode) and converting them into line-

112 of-sight (LOS) transmissions at each wavelength and tangent altitude. The species inversion
113 algorithm uses these multi-wavelength LOS transmission profiles to derive vertical profiles of
114 trace gas concentrations and aerosol extinction coefficients. This is done by first removing
115 modeled contributions from Rayleigh scattering and O₄ absorption, then separating the remaining
116 LOS transmission profiles into the contributions from each species of interest, and lastly
117 inverting these LOS contributions into vertical profiles of concentration or extinction using a
118 global fit inversion method (or a nonlinear Levenberg-Marquardt onion peeling method for water
119 vapor or temperature/pressure retrievals).

120 The solar occultation retrieval for SAGE III actually produces three separate ozone
121 products. The “MES” algorithm uses absorption features in the ultraviolet (<300 nm) to retrieve
122 vertical profiles between ~45 and ~100 km. The other two use ozone absorption in the Chappuis
123 band (near 600 nm) to retrieve vertical profiles from the surface or cloud top up to 70 km. Each
124 uses the same pixel groups in the spectral channel surrounding 600 nm (Channel 5) but differ in
125 how they treat aerosol and NO₂ within the retrieval. The “MLR” algorithm uses Channels 5 and
126 3 (~450 nm) to solve for both O₃ and NO₂ simultaneously while making an assumption about the
127 spectral shape of aerosol extinction through each channel. The “AO3” algorithm removes the
128 contributions from NO₂ that were solved in the MLR retrieval and then uses all of the data
129 between Channels 4 and 11 (see Figure 1), excluding the O₂ A-band and the H₂O channels, to
130 better constrain the influence of aerosol. The AO3 algorithm is similar to the retrieval used for
131 the SAGE II instrument (e.g., Chu et al., 1989; Damadeo et al., 2013). It is worth noting that
132 while the AO3 algorithm explicitly solves for aerosol extinction in each channel, this solution is
133 not reported. Instead, the reported aerosol is computed as a residual while using the MLR
134 solution for ozone and NO₂.

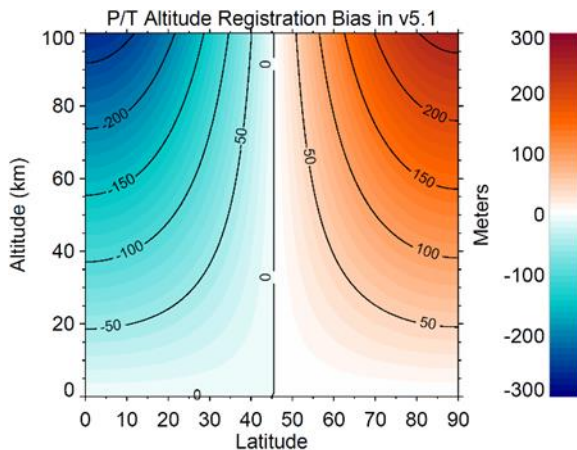
135 2.2 Known anomalies in version 5.1

136 The SAGE III/ISS instrument is by far the most/best characterized SAGE instrument.
137 The detailed knowledge of the intricacies of the instrument’s behavior and performance allow
138 the SAGE III team to incorporate several new algorithms to improve the data quality. One such
139 characterization is that of the spectral stray light within the spectrometer (reentrance spectra).
140 While the instrument was still on the ground, a thorough characterization of the spectral stray
141 light was performed on the instrument and one particular problem area was identified. A portion
142 of the light incident on the UV range of the CCD actually comes from near the peak of Chappuis
143 ozone absorption. This will have a negative impact on the mesospheric ozone retrieval and needs
144 to be corrected. While a rudimentary correction is currently implemented, it stems from an ad-
145 hoc correction derived for SAGE III/M3M data and does not use the most up-to-date
146 information. As such, we do not recommend the MES ozone product for validation or research
147 studies as it is still preliminary.

148 The SAGE III/ISS algorithm uses auxiliary temperature and pressure data from MERRA-
149 2 (Modern-Era Retrospective analysis for Research and Applications, version 2) (GMAO, 2015,
150 Gelaro et al., 2017), which is necessary for modeling refraction and molecular (Rayleigh)
151 scattering. These data are provided with geopotential heights, which the SAGE algorithm
152 converts to geometric altitudes at the location of the measurement. It has been discovered that
153 this conversion between geopotential height and geometric altitude, which was actually copied
154 from the SAGE II algorithm, was never thoroughly vetted and is more of an approximation (i.e.,
155 it assumes that the surface gravity is not latitude-dependent). As such, the current altitude

156 registration of the meteorological products that pass through the algorithm, but not the retrieved
 157 profiles of species concentrations or aerosol extinctions, are biased on the order of 100 or so
 158 meters (altitude and latitude dependent) as shown in Figure 2 (see the Appendix for a
 159 recommended correction). The impact of this mis-registration would be most noticeable when
 160 converting SAGE III retrieved ozone from native number density on geometric altitude to
 161 mixing ratio on pressure (VMR/P) coordinates when using the reported temperatures and
 162 pressures in the SAGE data files, especially at higher altitudes (see Appendix). It is, of course,
 163 also noteworthy to point out that, since the code was present in the SAGE II v7.0 algorithm, that
 164 data product has a similar bias when making the same conversion to VMR/P coordinates.

165



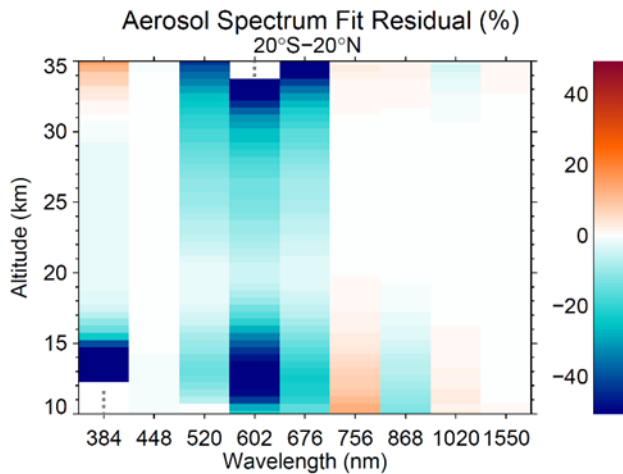
166

167 **Figure 2:** Estimated altitude registration errors in the reported SAGE III/ISS (v5.1) auxiliary
 168 temperature and pressure data.

169 Since aerosol measurements are intertwined with ozone measurements (i.e., through
 170 partitioning of the slant-path transmissions into the contributions from ozone, aerosol, and other
 171 interfering gases), assessing the quality of the aerosol product can also yield information about
 172 the quality of the ozone product. While aerosol extinctions at different wavelengths will vary
 173 with atmospheric conditions (e.g., total amount and type of aerosol from volcanoes and/or fires),
 174 it is expected that the “aerosol spectrum” (i.e., extinction as a function of wavelength) should be
 175 slowly varying and monotonic in almost all stratospheric conditions (Thomason et al., 2010).
 176 Instead, the aerosol spectrum derived from SAGE III/ISS measurements exhibits a “dip” near
 177 600 nm that has different characteristics in different altitude regimes (latitude-dependent) as
 178 shown in Figure 3. At altitudes in the troposphere and lowermost stratosphere (below ~20 km in
 179 the tropics), this dip follows the shape of the ozone cross-sections and is systematically larger at
 180 lower altitudes. The primary contribution appears to be an error in the creation of the
 181 spectroscopic database for O₄ used by the retrieval algorithm (i.e., a preprocessing error, not an
 182 error in the source cross-sections themselves). This yields the incorrect spectroscopic shape of
 183 O₄, which aliases into the retrieval and results in a solution for ozone that should be too large
 184 (discussed later) when the contribution to extinction from O₄ is significant (i.e., scales with
 185 density squared). Since aerosol is solved as a residual using MLR ozone, any systematically
 186 large ozone would cause systematically small aerosol showing a wavelength-dependence that
 187 scales with the ozone cross-sections. At altitudes above the lowermost stratosphere (≥ 20 km in
 188 the tropics), this dip still follows the shape of the ozone cross-sections but scales with the ozone

189 mixing ratio. A possible explanation for this is that the overall magnitude of the source ozone
 190 cross-section database is too large by 1–2% percent in the Chappuis relative to the other
 191 channels, but this requires further study. It is noteworthy that the magnitude of the dips is smaller
 192 in the aerosol data produced by the AO3 algorithm (not shown). This suggests that the use of
 193 additional aerosol channels in the retrieval better constrains the allowable shape of the aerosol
 194 spectrum, resulting in a potentially more robust aerosol data product. The SAGE team is
 195 investigating if the aerosol solution from the AO3 algorithm should be the released data product
 196 in future versions.

197



198

199 **Figure 3:** Residuals of a quadratic fit to the aerosol spectrum in log-log space using the aerosol
 200 extinctions at 448, 756, 868, 1020, and 1550 nm. The residuals are the median relative residuals
 201 of all SAGE III/ISS data from June 2017 to May 2019 between 20°S and 20°N. Results at mid-
 202 latitudes are similar, simply shifted down in altitude. Grey stippling denotes areas where aerosol
 203 extinction data does not exist. The median residuals in the channels used for the quadratic fit are
 204 <1% between ~20–30 km.

205 3 Correlative satellite and ground based ozone datasets

206 3.1 Aura MLS

207 The Earth Observing System (EOS) Microwave Limb Sounder (MLS) aboard the Aura
 208 satellite has provided daily global measurements of ozone (O_3) profiles and other trace gases
 209 from the upper troposphere to the upper mesosphere from August 2004 to present. Aura MLS
 210 measures thermal radiance emissions in 5 broad regions between 118 GHz and 2.5 THz by
 211 scanning the Earth's atmospheric limb vertically from the ground to ~90 km (Waters et al.,
 212 2006). Aura is in a sun-synchronous near-polar orbit with ascending equatorial crossing time of
 213 ~13:45 LT. Unlike the UARS MLS instrument, which observed limb emission in a direction
 214 perpendicular to the spacecraft flight direction, Aura MLS observes emission from the
 215 atmosphere directly ahead of the satellite. This results in near global-coverage from both daytime
 216 and nighttime measurements with ~3500 profiles each day.

217 Aura MLS ozone retrieved from the 240 GHz spectral region by using an optimal
 218 estimation approach (Rodgers, 2000; Livesey et al., 2006) is the standard reported ozone

219 product. It has a vertical resolution of 2.5–3 km from the upper troposphere to the lower
220 mesosphere, and ~5 km in the upper mesosphere. As indicated by comparisons with correlative
221 measurements, the estimated accuracy of MLS v2.2 ozone is within about 5% for much of the
222 stratosphere. The biases increase with decreasing altitudes, with some systematic positive biases
223 of 10–20% in the lowest portion of the stratosphere (Froidevaux et al., 2008; Livesey et al.,
224 2008) and ~20–30% in the upper troposphere (Jiang et al., 2007).

225 The latest Aura MLS v4.23 ozone data were used in this study. MLS v4.2x ozone profiles
226 are very similar to v2.2 in the stratosphere and above, so the validation results for v2.2 product
227 generally hold for the v4.2x product (Livesey et al., 2018). MLS v4.2x ozone profiles are
228 retrieved on 12 surfaces per decade between 316 hPa and 1 hPa, twice as fine a resolution as that
229 used in v2.2. There are several improvements in MLS v4.2x ozone retrievals. The high bias of
230 MLS v2.2 ozone at 215 hPa is reduced in v4.2x. Compared to v3.3 ozone, v4.2x reduces the
231 vertical oscillation behavior in the tropical upper troposphere and lower stratosphere (UT/LS)
232 regions (although some oscillations still exist). The sensitivity of retrieved ozone to thick clouds
233 is also improved in the v4.2x product. In this study, MLS v4.2x ozone data were screened based
234 on the recommendations of Livesey et al. (2018).

235 3.2 OSIRIS

236 The Optical Spectrograph and InfraRed Imaging System (OSIRIS) on board the Odin
237 satellite has been taking limb scattered measurements of the atmosphere from November 2001 to
238 present. It operates at wavelengths of 280–810 nm, with a spectral resolution of ~1 nm
239 (Llewellyn et al., 2004; McLinden et al., 2012). The Odin satellite has a polar orbit with
240 equatorial crossing local times at ~6:00 PM (ascending node), and at 6:00 AM (descending
241 node). OSIRIS can provide near global coverages (up to 82°) near the equinoxes, sunlit summer
242 hemisphere and no coverage of mid to high latitude winter hemisphere.

243 The OSIRIS SaskMART v5.0x ozone data are retrieved using the multiplicative algebraic
244 reconstruction technique (MART) (Degenstein et al., 2009; Roth et al., 2007), and the
245 SASKTRAN spherical radiative transfer model (Bourassa et al., 2008, Zawada et al., 2015). The
246 retrieval algorithm simultaneously uses and merges information from UV and VIS radiances.
247 Ozone number density, NO₂, aerosol extinctions and albedo are retrieved from 60 km down to
248 cloud tops (or 10 km during absence of clouds) with a vertical resolution of ~2 km at low
249 altitudes. The resolution decreases toward higher altitudes and reaches ~3 km at 50 km.

250 Through inter-comparisons with other satellite and in-situ measurements, the OSIRIS
251 ozone data show good agreement (within 5%) with correlative measurements for altitudes above
252 20 km. Between 20 km and the tropopause OSIRIS shows negative biases of ~5–20% for
253 latitudes between 40°S and 40°N (Adams et al., 2014). It was also found that OSIRIS ozone
254 biases depend on the OSIRIS optics temperature, retrieved aerosols, and albedo. The latest
255 OSIRIS v5.10 ozone data, with a drift correction of sensor pointing bias, are used in this study.
256 The drift in previous OSIRIS v5.07 ozone data (Hubert et al., 2016) is attributed to a changing
257 bias in the procedure to determine the tangent altitudes of limb radiance profiles (Bourassa et al.,
258 2018). There is no further filtering applied to OSIRIS data in this study since the OSIRIS v5.10
259 ozone profiles have been screened for outliers, based on the techniques described by Adams et
260 al. (2013), prior to its distribution to the public.

261 3.3 ACE-FTS

262 The Atmospheric Chemistry Experiment – Fourier Transform Spectrometer (ACE-FTS)
263 is a solar occultation instrument that records spectra between 2.2 and 13.3 μm ($750\text{--}4400\text{ cm}^{-1}$)
264 at a high spectral resolution of 0.02 cm^{-1} (Bernath et al., 2005, 2017). ACE-FTS was launched
265 on the SCISAT satellite in August 2003. Measurements are taken during each sunrise and sunset
266 per orbit. ACE-FTS measurements are taken up to 30 times per day at sunrise and sunset. The
267 volume mixing ratios of ozone and other trace gases as well as temperature and pressure are
268 retrieved from cloud tops to $\sim 100\text{ km}$ by a modified global fit approach based on the Levenberg-
269 Marquardt nonlinear least-squares method (Boone et al., 2005). The final results are provided on
270 the measurement (tangent height) grid, with vertical resolution of 3–4 km, and interpolated to a 1
271 km interval using a piecewise quadratic method.

272 When compared with Michelson Interferometer for Passive Atmospheric Sounding
273 (MIPAS) and Aura MLS, the ACE-FTS v3.5 ozone generally agree within 5% in the middle
274 stratosphere ($\sim 20\text{--}45\text{ km}$), and exhibit a positive bias of $\sim 10\text{--}20\%$ in the upper stratosphere and
275 lower mesosphere (Sheese et al., 2017). ACE-FTS also tends to show negative bias with respect
276 to MIPAS and MLS below 20 km. The negative bias increases with decreasing altitudes, and
277 reaches $\sim 20\text{--}30\%$ near 10 km.

278 The ACE-FTS version 3.5 data extend from Feb. 2004 to March 2013. A new version
279 number (version 3.6) is used for data onward when the version 3.5 processor was ported from a
280 Unix to Linux based system. Although the ACE-FTS team just released version 4.0 data, we
281 used version 3.6 data because version 3.5/3.6 data are still the recommended data set for
282 scientific and validation studies at the time of writing. Data quality flags based on Sheese et al.
283 (2015) are provided in version 3.5/3.6 netCDF files. All ACE-FTS data with a non-zero flag
284 value were excluded from this study (ACE-FTS data usage guide and file description, 2017).

285 3.4 OMPS LP

286 The Ozone Mapping and Profiler Suite (OMPS) was launched in October 2011 on board
287 the Suomi National Polar-orbiting Partnership (NPP) satellite. OMPS consists of three ozone-
288 acquiring sensors (Flynn et al., 2006) designed to provide profile and total ozone measurements.
289 All three sensors measure scattered solar radiances in overlapping spectral ranges and scan the
290 same air masses within 10 min (Kramarova et al., 2014). The nadir module combines two
291 sensors, the Total Column Nadir Mapper (TC-NM) for measuring total column ozone and the
292 Nadir Profiler (NP) for ozone vertical profiles. The Limb Profiler (LP) module is designed to
293 measure vertical profiles of ozone with higher vertical resolution ($\sim 2\text{--}3\text{ km}$) from the upper
294 troposphere to the mesosphere. In this study, we will use OMPS ozone profile products from the
295 Limb Profiler (OMPS LP).

296 The OMPS LP sensor is based on principals tested in the 1990s by flying the Shuttle
297 Ozone Limb Sounding Experiment on two space shuttle missions, STS-87 and STS-107 (Flittner
298 et al., 2000; McPeters et al., 2000). OMPS LP measures solar radiances scattered from the
299 atmospheric limb in UV and VIS spectral ranges to retrieve ozone profiles with a high vertical
300 resolution. The OMPS LP algorithm retrieves ozone profiles independently from UV and VIS
301 measurements using wavelengths pairs in the UV range and triplets in the VIS range (Rault and
302 Loughman, 2013). Measured radiances are first normalized with radiances measured at 55.5 km
303 and 40.5 km for UV and VIS retrievals respectively. In this study we use the most recent version

304 2.5 that was described and validated in Kramarova et al. (2018). Comparisons of ozone profiles
305 derived from OMPS LP with MLS, OSIRIS and ACE-FTS demonstrated that between 18 and 42
306 km the mean biases are within $\pm 10\%$, with the exception of the northern high latitudes where
307 larger negative biases are observed between 20 and 32 km due to a thermal sensitivity issue
308 (Kramarova et al., 2018). In the upper stratosphere and lower mesosphere (> 43 km) OMPS LP
309 tends to have a negative bias against Aura MLS, ACE-FTS and OSIRIS instruments. In the
310 UTLS below 15–18 km, especially in the tropics, negative biases increase up to $\sim 30\%$. A
311 positive drift of 0.5% yr⁻¹ against MLS and OSIRIS was found that was more pronounced at
312 altitudes above 35 km. Such a pattern is consistent with a possible 100 m drift in the LP sensor
313 pointing detected in the analysis of LP radiances (Kramarova et al., 2018).

314 3.5 Ozonesondes

315 Ozonesondes are balloon-borne in situ instruments that can provide ozone profiles from
316 the surface to the middle atmosphere (~ 30 – 35 km) with a high vertical resolution (~ 100 – 150 m).
317 When standard operating procedures are followed, the three most commonly used sonde types
318 produce consistent results. For altitudes between the tropopause and ~ 28 km, the systematic
319 biases are less than 5% with precision better than 3% (Smit and ASOPOS panel, 2014). At
320 higher and lower altitudes, the ozonesonde data quality degrades and the differences between
321 different sonde types become larger. In the troposphere, the ECC type sondes have the best
322 quality with estimated accuracy of 5–7 % and a precision of 3–5 % (Smit and ASOPOS panel,
323 2014). Ozonesonde data from the Southern Hemisphere Additional Ozonesondes (SHADOZ)
324 network (Witte et al., 2017; Thompson et al., 2017), World Ozone and Ultraviolet Radiation
325 Data Center (WOUDC, <https://woudc.org>), and National Oceanic & Atmospheric Administration
326 (NOAA) (<https://www.esrl.noaa.gov/gmd/ozwv/ozsondes/>) are used to evaluate the SAGE
327 III/ISS data. Ozonesonde stations used in this study can be seen in Table 1 in section 5.3.

328 3.6 Stratospheric ozone lidar

329 The Differential Absorption Lidar (DIAL) is a powerful technique to measure the vertical
330 distribution of ozone in the stratosphere and troposphere with a vertical resolution of several
331 hundred meters near tropopause to 3–5 km in the upper stratosphere (Godin et al., 1999). This
332 technique uses two (or more) laser wavelengths which are chosen such that one has strong ozone
333 absorption and the other has much lower absorption. The concentration of ozone is retrieved by
334 measuring the different absorptions of the backscatter data at two wavelengths. The choice of
335 selected laser wavelengths depends on whether the measurement is intended for the troposphere
336 or stratosphere (Megie et al., 1985).

337 We used stratospheric ozone lidars in the Network for the Detection of Atmospheric
338 Composition Change (NDACC, <http://www.ndacc.org>), which provide ozone number density vs
339 geometric altitude profiles between the tropopause and 45–50 km. The precision of NDACC
340 ozone lidar is $\sim 1\%$ up to 30 km, 2–5% at 40 km and 5–25% at 50 km (Keckhut et al., 2004).
341 Intercomparisons of different processing algorithms within the NDACC network indicate that the
342 biases in retrieved ozone are $\sim 2\%$ for altitudes between 20 and 35 km, and increase to ~ 5 – 10% at
343 other altitudes (Keckhut et al., 2004). Those larger biases are due to lower signal to noise ratio or
344 saturation of the detectors. By comparing lidars with ozonesondes and satellites, Nair et al.
345 (2012) also showed biases less than $\pm 5\%$ in the lidar for altitudes between 20 and 40 km. We

346 used data from five stratospheric ozone lidars in the NDACC networks (Table 2) that provide
347 overlapping data with SAGE III/ISS in this study.

348 **4 Methodology**

349 To evaluate the quality of SAGE III/ISS ozone data with correlative measurements, we
350 need to consider uncertainties from (1) spatial/temporal differences (mismatch), (2) different
351 horizontal and vertical resolutions (smoothing), and (3) converting ozone profiles to different
352 coordinates (auxiliary) (von Clarmann, 2006; Hubert et al., 2016). Common coincidence criteria
353 are used to minimize the effect of spatial and temporal differences (i.e., mismatch error) between
354 SAGE III/ISS and correlative measurements. For satellite comparisons, coincident profiles need
355 to be on the same date with latitude difference less than $\pm 2^\circ$ and distance between them less than
356 1000 km. When there is more than one correlative ozone profile with a SAGE III/ISS ozone
357 profile, the closest one in space is used. For comparisons with ground-based measurements,
358 larger coincidence criteria are used, with temporal differences of ± 24 hours, and spatial
359 differences of $\pm 5^\circ$ in latitude and distance less than 1000 km. The larger coincidence criteria for
360 ground-based measurements is to ensure there are enough correlative data to characterize the
361 bias and precision of SAGE III ozone while minimizing the effects due to temporal and spatial
362 variabilities

363 There is no good way to minimize the effect of different horizontal resolutions between
364 instruments (e.g., satellite measurement vs ozonesondes); the ozone profiles from instruments
365 with finer vertical resolution, however, can be smoothed before comparison to minimize the
366 biases due to different vertical resolutions. For comparisons between SAGE III and MLS, the
367 SAGE III ozone profiles were interpolated to MLS levels by using a least squares linear fit
368 method recommended by the MLS science team (Livesey et al., 2018). The MLS averaging
369 kernels and a priori profiles were not applied to interpolated SAGE III ozone profiles (e.g.,
370 Rodgers and Connor, 2003), because the effect of further smoothing by applying MLS averaging
371 kernels has been shown to be very small (e.g., Adams et al., 2014). This is because the MLS
372 averaging kernels are close to delta functions (sharply peaked and with vertical resolution
373 comparable to the MLS retrieved profile level spacing). Finally, the MLS and SAGE III ozone
374 number density profiles at varying geometric altitudes were linearly interpolated to every 1 km
375 interval.

376 ACE-FTS ozone has a vertical resolution of $\sim 3\text{--}4$ km. Ozone data are retrieved at tangent
377 altitudes, with vertical spacing of ~ 1.5 km at lower altitudes increasing to ~ 6 km in the
378 mesosphere. Retrieved ozone profiles are then interpolated to a 1 km interval by using a
379 piecewise quadratic method. To minimize the effect of different vertical resolutions, the SAGE
380 III/ISS ozone profiles were first smoothed at ACE-FTS retrieved tangent altitudes by using a
381 weighted Gaussian distribution function with a full width half maximum (FWHM) that
382 approximates the vertical resolution of ACE-FTS (Kar et al., 2007; Sheese et al., 2017). The
383 smoothed SAGE III ozone profiles were subsequently interpolated to a 1 km grid before
384 comparing with ACE-FTS data. Alternatively, the SAGE III ozone profiles can be smoothed by a
385 triangular function with full width at the bases equal to the vertical resolution of ACE-FTS
386 (Dupuy et al., 2009). It has been found that the choice of smoothing function (e.g., triangular or
387 Gaussian function) does not introduce systematic bias when comparing ozone profiles with
388 different vertical resolutions although it may introduce a slight difference in random errors
389 (Hubert et al., 2016). The OSIRIS and OMPS LP have similar vertical resolutions of ~ 2 km in

390 most of stratosphere and ~3 km in the upper stratosphere and lower mesosphere. Similarly, the
 391 SAGE III ozone profiles were smoothed by the Gaussian distribution with FWHM corresponding
 392 to the vertical resolution of OSIRIS and OMPS LP. The ground-based ozonesondes and lidar (in
 393 the UT/LS regions) have better vertical resolution than SAGE III. Correlative ozone profiles
 394 from ozonesondes and lidar, therefore, were smoothed according to the SAGE III resolution (~1
 395 km) before further inter-comparisons.

396 In order to compare collocated ozone profiles between SAGE III/ISS and correlative
 397 measurements, those profiles need to be on the same coordinate. Due to an altitude registration
 398 error in current SAGE III/ISS v5.1 temperature and pressure data (see discussion in section 2),
 399 we used ozone in the SAGE III native retrieval coordinate, number density on geometric altitude.
 400 Ozone profiles in different coordinates (e.g., mixing ratio on pressure or mixing ratio on
 401 geometric altitude) from Aura MLS, ACE-FTS and ozonesondes were converted to SAGE III
 402 native coordinates by using their own observed temperature data, except for Aura MLS.
 403 Although Aura MLS also measures temperatures and retrieves geopotential heights (GPH) along
 404 with each ozone profile, there are seasonally and latitudinally-repeating systematic errors in GPH
 405 (Livesey et al., 2018). The assimilated meteorology fields from the second Modern-Era
 406 Retrospective analysis for Research and Applications (MERRA-2) (GMAO, 2015), therefore,
 407 were used. The MERRA-2 temperatures (with resolution of 0.625° in longitude, 0.5° in latitude,
 408 72 model layers from surface to 0.01 hPa, and every 3 hours), were first interpolated to MLS
 409 locations and pressure levels. The geopotential heights (GPH) at MLS pressure levels were then
 410 derived by using the hypsometric equation and reference altitude from MERRA-2. With
 411 interpolated MERRA-2 temperatures and geopotential heights corresponding to the MLS grid,
 412 the original MLS ozone profiles can be converted to number densities on geometric altitudes.

413 To assess the overall quality of SAGE III/ISS ozone data with correlative measurements,
 414 we use the following two metrics: the mean relative differences and the standard deviations of
 415 relative differences. The mean bias (relative difference), $\overline{D(z)}$, in percentage is defined as

$$\overline{D(z)} = 100 \times \frac{1}{n(z)} \sum_{i=1}^{n(z)} \frac{x_i^s(z) - x_i^c(z)}{x_i^c(z)}$$

416 where $n(z)$ is the number of coincident profiles, $x^s(z)$ and $x^c(z)$ are ozone number density at a
 417 particular altitude (z) from SAGE III and correlative measurement, respectively. The SAGE III
 418 reported uncertainty along with retrieved ozone contains random errors from three primary
 419 sources: (1) line-of-sight optical depth measurement error, (2) estimated Rayleigh scattering, and
 420 (3) uncertainty associated with removal of contributions from interfering gases and aerosol
 421 (SAGE III ATBD, 2002). In order to verify SAGE III reported random errors and provide
 422 additional information regarding the significance of the bias and the upper limit of the precision
 423 of SAGE III/ISS ozone data, we calculate the standard deviation of bias-corrected differences.
 424 The de-biased standard deviation is a measure of the combined precision of instruments that are
 425 being compared (von Clarmann, 2006), and is represented as

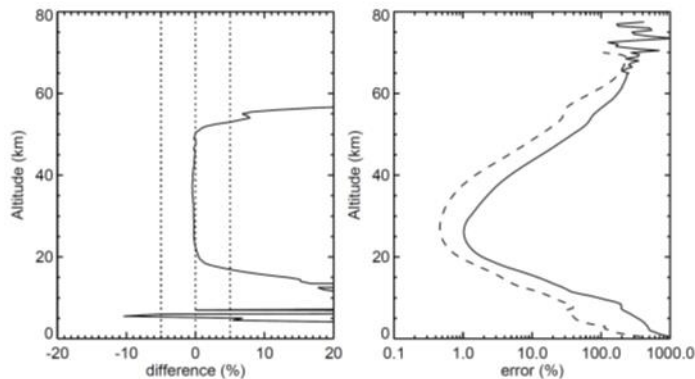
$$\sigma(z) = \sqrt{\frac{1}{(n(z) - 1)} \sum_{i=1}^{n(z)} (D_i(z) - \overline{D(z)})^2}$$

426 where $n(z)$ is the number of coincidences, $D_i(z)$ is the relative difference for the i th coincident
 427 pair, and $\overline{D(z)}$ is the mean relative difference at a particular altitude (z).

428 5 Results

429 5.1 Comparisons of the SAGE III/ISS solar ozone between AO3 and MLR algorithms 430 and between sunrise and sunset measurements

431 As mentioned earlier in section 2, SAGE III/ISS produces two solar ozone products based
 432 on the ozone absorption in the Chappuis band by two different retrieval algorithms. The mean
 433 differences and reported uncertainties from these two ozone products are shown in Figure 4. The
 434 mean differences between AO3 and MLR ozone are negligible between 20 and 50 km, but
 435 become larger toward higher or lower altitudes. For altitudes above 50 km, the MLR ozone
 436 shows increasing high biases, reaching ~ 20 – 30% at 60 km. In the lower stratosphere below 20
 437 km the MLR ozone also shows increasing high biases (with decreasing altitudes), as large as
 438 $\sim 20\%$ at 10 km. As expected both MLR and AO3 ozone show the smallest uncertainties around
 439 the ozone peak area. The uncertainties become larger toward higher and lower altitudes where
 440 there is less ozone or larger contributions from other interfering trace gases and aerosol in the
 441 retrieval algorithms. The reported uncertainties in MLR ozone are a few percent between 20 and
 442 30 km. They become larger than 100% for altitudes above ~ 55 km and below 10 km. The mean
 443 uncertainties in AO3 ozone are approximately 2–3 times smaller than those of MLR ozone.



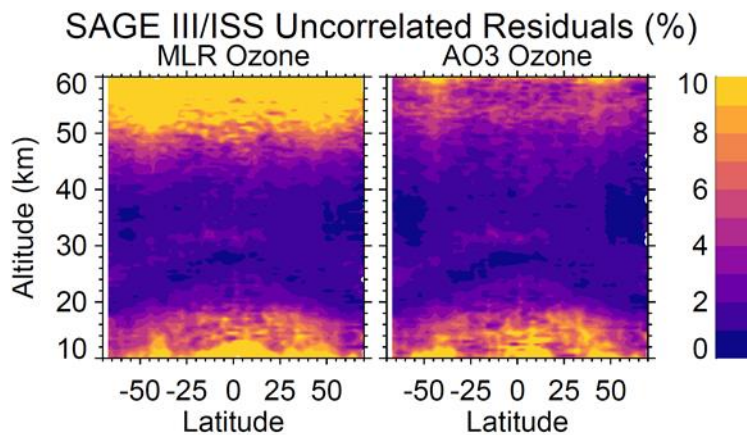
444

445 **Figure 4:** Mean relative differences between SAGE III/ISS MLR and AO3 solar ozone data
 446 (left). Percentage differences are represented as $(\text{MLR}-\text{AO3})/\text{AO3} \times 100\%$. Mean reported
 447 uncertainties in MLR (solid) and AO3 (dashed line) ozone profiles (right). Mean differences and
 448 uncertainties are based on all retrieved ozone profiles between June 2017 and May 2019.

449 By using the residual analysis detailed in Damadeo et al. (2014), we can get an
 450 assessment of random errors in AO3 and MLR ozone. The time series of observed ozone
 451 (averaged within a specific temporal/spatial window) contains information about the natural
 452 variability and instrument uncertainties. The natural variability of ozone can be approximated by
 453 a regression model with predictors for seasonal cycle, long term trend, quasi-biennial oscillation
 454 (QBO), solar cycle, etc. The spread of the residuals from the regression of observed ozone data
 455 can be used to ascertain the quality of the regression model and observed data itself. The total
 456 residuals consist of the correlated and uncorrelated residuals. The correlated residuals come from
 457 autocorrelation within the data and typically represent the natural variability that is not well

458 represented by the regression model. Uncorrelated residuals represent a combination of
 459 measurement uncertainty and geophysical variability that is not well-sampled (e.g., zonal
 460 variability within the daily zonal means used for this analysis). For the purpose of this validation
 461 study, we only care to look at the uncorrelated residuals as an indication of data quality or
 462 precision. Since the choice of regression model has little bearing on the uncorrelated residuals, a
 463 rather simplistic model consisting only of a seasonal cycle was used for this analysis, applied to
 464 all SAGE III/ISS data between June 2017 and May 2019.

465 The spreads of the uncorrelated residuals from the regression of AO3 and MLR ozone are
 466 shown in Figure 5, which can provide an estimate of the upper limit of uncertainties in both
 467 datasets. This is an upper limit because zonal variability within each daily zonal mean used for
 468 this analysis will also increase the uncorrelated residuals. However, since the sampling is
 469 identical between the two data products, a direct comparison of the uncorrelated residuals yields
 470 information about the intrinsic data quality of each data product independent of any correlative
 471 source instrument. We can see that the uncorrelated residuals are similar throughout most of the
 472 stratosphere between the two products ($\sim 1\text{--}3\%$). The MLR ozone, however, is significantly
 473 noisier than the AO3 product both in the upper-most stratosphere and mesosphere as well as in
 474 the lowermost stratosphere and troposphere. These results are similar to those from a study
 475 (Wang et al., 2006) of SAGE III/M3M data using comparisons with other correlative data sets.
 476 While useful as an independent comparison of the relative data quality of the two data products,
 477 evaluating the statistics of the uncertainties (or precisions) for individual profiles via
 478 comparisons of correlative measurements can help mitigate the impact of the dynamical
 479 variability in the regression sample size (i.e., a daily zonal mean) and will be evaluated in later
 480 sections.

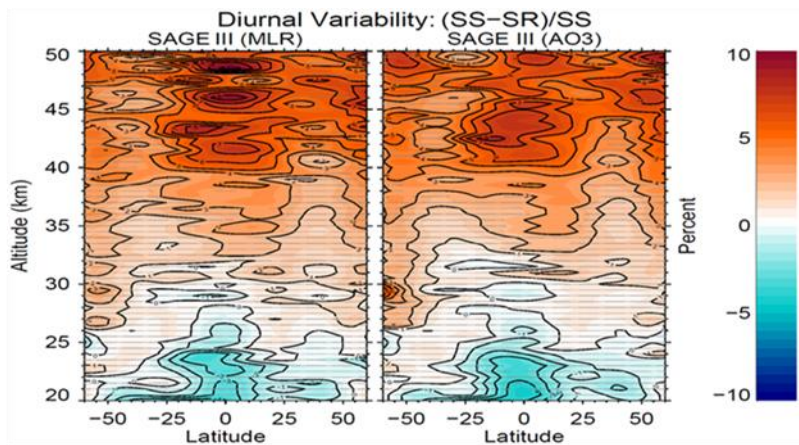


481
 482 **Figure 5:** Standard deviations of the uncorrelated residuals in percentage as a function of latitude
 483 and altitude from the regression of SAGE III/ISS MLR (left) and AO3 (right) ozone data.

484 It has been reported that there is a difference in observed ozone values between sunrise
 485 and sunset from solar occultation instruments (Wang et al., 1996; Brühl et al., 1996; Kyrölä et
 486 al., 2013; Sakazaki et al., 2015). Measurements from the Halogen Occultation Experiment
 487 (HALOE), ACE-FTS, and Superconducting Submillimeter-Wave Limb-Emission Sounder
 488 (SMILES) show that the sunset values are higher than sunrise by 3–5% between 40 and 50 km
 489 (Sakazaki et al., 2015). SAGE II shows similar features as HALOE, ACE-FTS and SMILES, but
 490 the magnitude of sunrise/sunset differences is approximately twice as large as those from other

491 satellites, especially in the tropics during January (Wang et al., 1996). Based on observations
 492 from SMILES and the Specified Dynamic version of the Whole Atmosphere Community
 493 Climate Model (SD-WACCM), Sakazaki et al. (2013, 2015) attributes the observed
 494 sunrise/sunset differences in the upper stratosphere to the vertical transport of atmospheric tidal
 495 winds, which reach a maximum in the tropics and during the winter season (Dec. to Feb.). The
 496 reason for the larger sunrise/sunset differences in SAGE II is not clear, but it is worth
 497 investigating whether a similar situation occurs in the SAGE III/ISS ozone data.

498 To investigate the sunrise/sunset differences in SAGE III/ISS retrieved ozone, we used
 499 two different methods. The first one is to apply the regression model described in Damadeo et al.
 500 (2018) to both SAGE II and SAGE III/ISS data simultaneously to derive the mean difference
 501 between sunrise and sunset data. There is currently insufficient sampling orthogonality within
 502 the SAGE III/ISS data set to differentiate seasonal variability from diurnal variability, so
 503 including SAGE II data (given its own diurnal cycle) helps constrain this. The lack of overlap
 504 between the two data sets is accounted for by considering SAGE III/ISS as an extension of the
 505 SAGE II product, which is acceptable since we are not interested in trend results in this work.
 506 The results are shown in Figure 6. Both AO3 and MLR ozone show similar results, with sunset
 507 values higher than sunrise by ~ 5 – 10% in the upper stratosphere, though the pattern of differences
 508 is more coherent for the AO3 product than the MLR product. The sunrise values, however,
 509 become slightly larger than sunset in the lower stratosphere below 25 km. The sunrise/sunset
 510 differences are also larger in the tropics than mid-latitudes. The vertical and latitudinal
 511 distributions of sunrise/sunset differences are consistent with the dynamical variations from
 512 atmospheric tidal winds (Sakazaki et al., 2013, 2015).

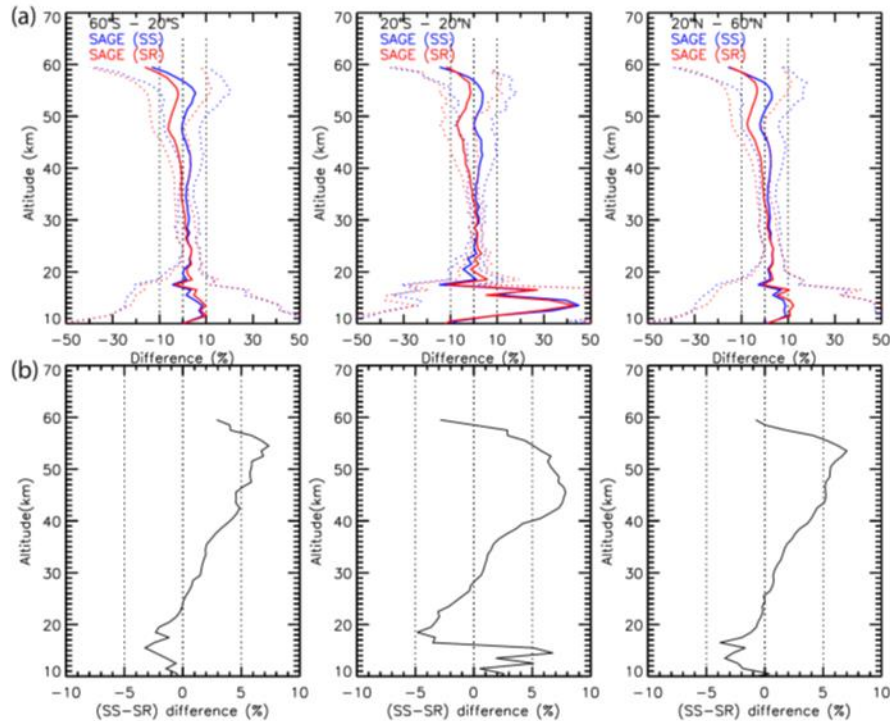


513

514 **Figure 6:** Mean differences between SAGE III/ISS sunrise (SR) and sunset (SS) ozone values
 515 from regression model analysis. Results from both MLR (left) and AO3 (right) algorithms are
 516 shown. The percentage difference is expressed as $(SS-SR)/SS \times 100\%$. The stippling denotes
 517 regions that are not statistically significant at the 2-sigma level.

518 We also used Aura MLS as transfer standard to evaluate the differences between SAGE
 519 III/ISS sunrise and sunset measurements. Figure 7 shows comparison results between SAGE
 520 III/ISS AO3 ozone, separated by sunrise or sunset, and coincident Aura MLS nighttime
 521 measurements. As shown in Figure 7, SAGE III/ISS sunset values are systematically higher than
 522 sunrise values by ~ 5 – 8% for altitudes between 40 and 55 km. In the lower stratosphere between
 523 the tropopause and ~ 25 km, the sunrise values become slightly larger (less than 5%) than sunset

524 values. Similar results were also found by using MLR ozone compared against collocated Aura
 525 MLS data, or comparing sunrise and sunset measurements directly (e.g., Wang et al., 1996) when
 526 they were observed on the same dates and approximately at the same locations (e.g., $\pm 1^\circ$ latitude,
 527 $\pm 5^\circ$ longitude, figures not shown). The reason for the large sunrise/sunset difference in SAGE
 528 retrieved ozone in the upper stratosphere is not clear, but since it occurs in both SAGE II and
 529 SAGE III/ISS, it could relate to the retrieval algorithm and needs further investigation.

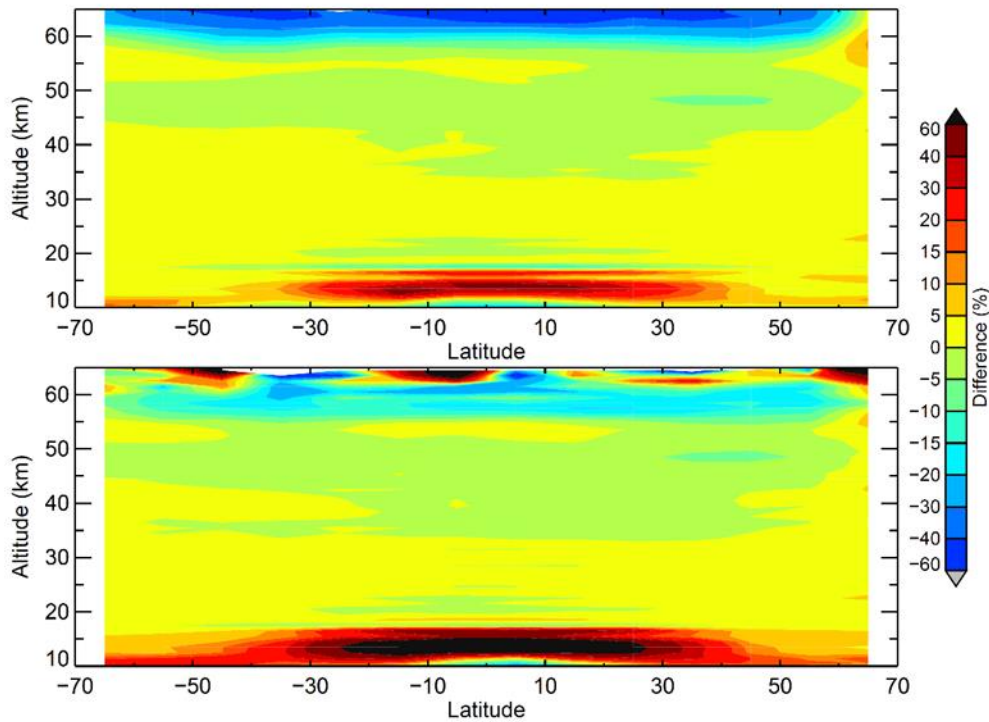


530

531 **Figure 7:** (a) The mean percentage differences (solid line) and standard deviations (dotted line)
 532 between SAGE III/ISS AO₃ ozone and coincident Aura MLS nighttime measurements between
 533 June 2017 and May 2019 in three latitude bands, 60°–20°S, 20°S–20°N, and 20°–60°N. The
 534 means and standard deviations of relative differences are separated into SAGE sunrise (red) and
 535 sunset (blue) data. (b) The relative differences between SAGE III/ISS sunrise and sunset
 536 measurements by using coincident Aura MLS as a transfer standard. The percentage difference is
 537 represented as $(SS-SR)/MLS \times 100$.

538 5.2 Comparisons between SAGE III/ISS and other satellites

539 Among the correlative satellite instruments, the Aura MLS provides the most
 540 comprehensive global coverages (from 82°S–82°N) each day with the equatorial crossing time at
 541 $\sim 1:45$ am and 1:45 pm. The comparisons between SAGE III/ISS retrieved stratospheric ozone
 542 products and Aura MLS nighttime measurements are shown in Figure 8. We used MLS
 543 nighttime measurements to minimize the effect of ozone diurnal cycle on the differences
 544 between SAGE III and MLS, since the SAGE III measurements occur during sunrise and sunset
 545 which in general yield ozone values that are closer to nighttime than daytime ozone (Takatoshi et
 546 al., 2013; Parrish et al., 2014).



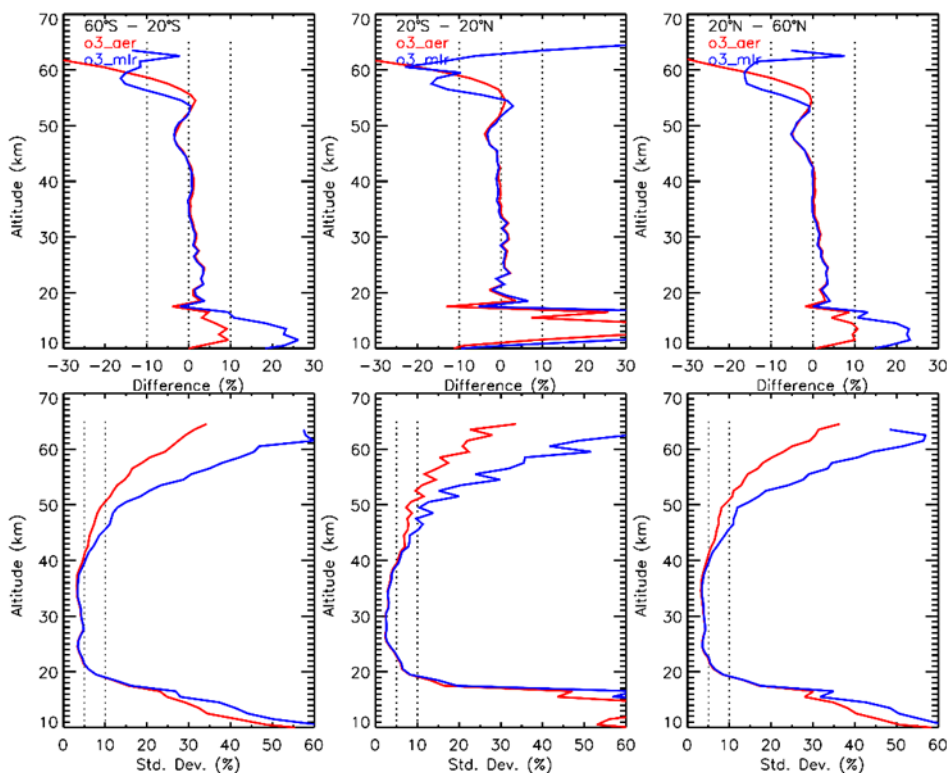
547

548 **Figure 8:** Mean differences between Aura MLS night time measurements and ozone retrieved
 549 from SAGE III/ISS AO3 (top) and MLR (bottom) algorithm as a function of latitude and
 550 altitude. Positive differences (in percentage) indicate the SAGE III/ISS ozone values are higher
 551 than Aura MLS.

552 SAGE III/ISS AO3 ozone shows very good agreement with Aura MLS for altitudes
 553 between ~20 and 55 km, with differences less than 5%. The differences become larger toward
 554 the lower stratosphere and upper troposphere and reach ~10% near the tropopause, with SAGE
 555 III ozone values higher than MLS. Above 55 km the SAGE III ozone values are systematically
 556 lower than those from Aura MLS with negative biases of ~10% at 60 km and 40–60% at 65 km.
 557 The larger biases (e.g., >40%) between SAGE III and Aura MLS in the mesosphere cannot be
 558 completely explained by the ozone diurnal cycle (e.g., sunrise/sunset vs nighttime) (Parrish et al.,
 559 2014). These biases could result from errors in the MERRA-2 temperature data in the
 560 mesosphere and/or deficiencies in SAGE III AO3 retrieval algorithm. We used MERRA-2 data
 561 to convert MLS ozone from mixing ratio and pressure coordinates to SAGE’s native number
 562 density and geometric altitude coordinates. Any systematic error in auxiliary temperature and
 563 pressure data can lead to errors in converted MLS ozone profiles, but the evaluation of MERRA-
 564 2 temperature data in the mesosphere is outside the scope of this paper. Since the SAGE III AO3
 565 ozone product is retrieved using the Chappuis band, the weakly attenuated signals in the
 566 mesosphere could yield degraded results in that region. Instead, the SAGE III/ISS MES
 567 algorithm may provide more information for mesospheric ozone after correcting for the stray
 568 light problem.

569 The SAGE III/ISS MLR ozone shows similar features as AO3 when compared against
 570 Aura MLS. The relative differences with MLS are less than 5% between 20 and 55 km for all
 571 latitudes. The differences, however, become larger at higher and lower altitudes. In the lower

572 mesosphere above 60 km, SAGE III MLR ozone shows positive biases of 20% or more for some
 573 latitudes. This is contrary to what is expected from the ozone diurnal cycle. SAGE III MLR
 574 ozone also shows positive biases in the lower stratosphere, with mean differences of
 575 approximately 10–30% in the middle to high latitudes and greater than 60% near the tropical
 576 tropopause.



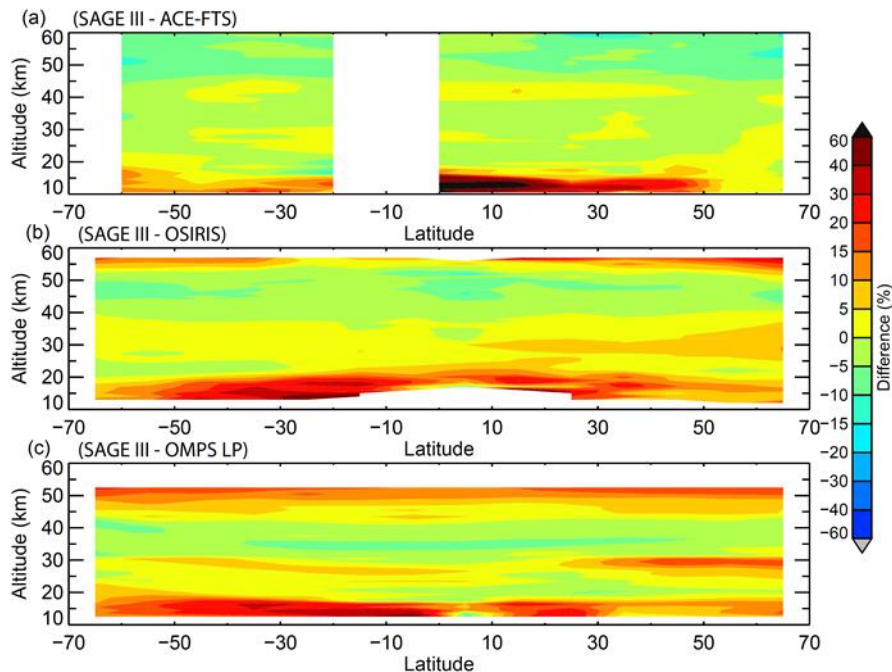
577

578 **Figure 9:** Mean differences (top panel) and standard deviations (bottom panel) between
 579 collocated Aura MLS and SAGE III/ISS ozone from AO3 (red) and MLR (blue) retrieval
 580 algorithm. Differences and standard deviations are derived in three broad latitude bands, 20°–
 581 60°S, 20°S–20°N, 20°–60°N, and represented as a percentage.

582 The mean relative differences and standard deviations between SAGE III/ISS AO3 and
 583 MLR ozone against Aura MLS are summarized in Figure 9. Between the two SAGE III retrieved
 584 solar ozone products, the AO3 shows overall better accuracy and precision than MLR ozone. The
 585 systematic biases in AO3 ozone are less than 3% from ~15 km to 55 km in the mid-latitudes and
 586 ~20 km to 55 km in the tropics. The biases increase with decreasing altitudes and reach ~10%
 587 near the tropopause. The differences between SAGE III AO3 and MLS also become larger for
 588 altitudes above 55 km due to an increase of the ozone diurnal cycle. The SAGE III/MLS
 589 differences oscillate with altitude in the lower stratosphere and upper troposphere (UT/LS)
 590 especially in the tropics. This mainly results from Aura MLS which reports ozone on a slightly
 591 finer vertical grid than its actual vertical resolution in that region (Livesey et al., 2018). SAGE
 592 III MLR ozone shows similar biases as AO3 for altitudes between 20 and 50 km, but the biases
 593 become larger outside those altitudes. This is consistent with the earlier results of direct
 594 comparisons between SAGE III AO3 and MLR ozone data (Figure 4). The MLR retrieved ozone
 595 also shows larger uncertainties than AO3 in the upper stratosphere and lower mesosphere (above

596 40 km) and in the UT/LS regions (below 20 km), as indicated by the larger standard deviations in
 597 Figure 9, which is consistent with results from the independent regression analysis shown in
 598 Figure 5. Similar features are also found in comparisons between SAGE III MLR ozone and
 599 other satellites (figures not shown). Because of the larger uncertainties and biases in MLR ozone
 600 for altitudes above 50 and below 20 km, we recommend using SAGE III AO3 ozone for
 601 scientific studies. In the following sections, we will just focus on validation results for SAGE III
 602 AO3 ozone.

603 The comparisons between SAGE III/ISS AO3 ozone and ACE-FTS, OSIRIS, OMPS LP
 604 are shown in Figure 10. Both SAGE III and ACE-FTS use solar occultation techniques to
 605 measure ozone. Due to limitation of the orbit geometry, there are no collocated SAGE III/ACE-
 606 FTS ozone profiles in the regions between equator and 20°S, and poleward of 60°S. The
 607 differences between SAGE III and ACE-FTS are in general within 5% between 15 and 45 km.
 608 Above 45 km SAGE III shows a negative bias of ~10%. Below 15–20 km, SAGE III values
 609 become larger than ACE-FTS by 10–20% in mid-latitudes (Figure 10a). This is consistent with
 610 an earlier study, which shows ACE-FTS v3.5 ozone has a positive bias of ~10–20% in the upper
 611 stratosphere and mesosphere (>45 km), and negative bias of 20–30% in the UT/LS (Sheese et al.,
 612 2017). SAGE III and OSIRIS show the best agreement between 20 and 50 km. The differences
 613 are generally within 5%, except in the northern hemisphere around 30 km, where the differences
 614 are slightly larger than 5% (Figure 10b). The reason for this hemispheric difference is not known
 615 but it doesn't occur in the comparisons between SAGE III against Aura MLS and ACE-FTS.

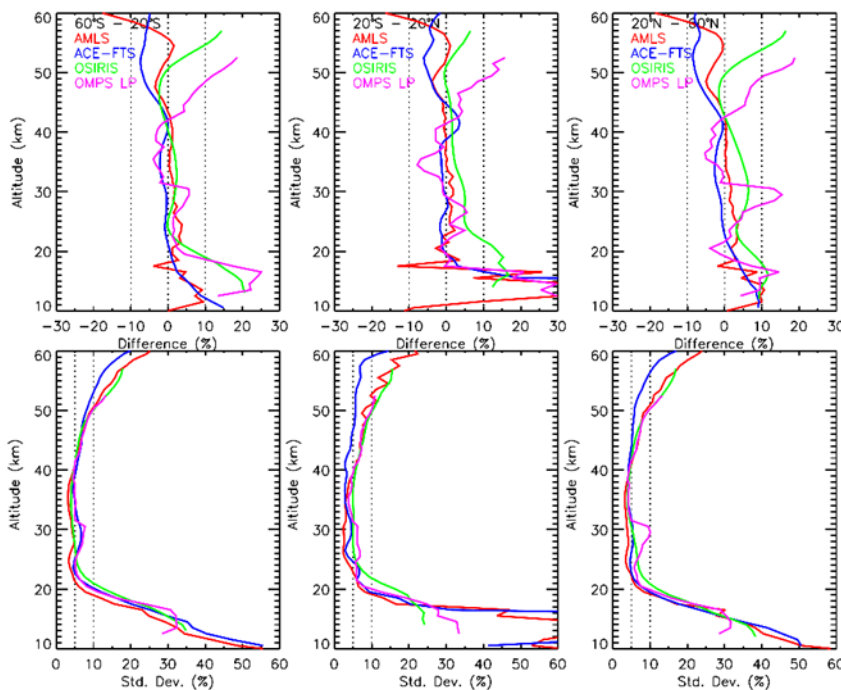


616

617 **Figure 10:** Mean differences between SAGE III/ISS AO3 ozone and correlative (a) ACE-FTS
 618 (b) OSIRIS and (c) OMPS LP measurements. Differences are represented as (SAGE-
 619 other)/other* 100%.

620 We can see that all satellite measurements show very good agreement, with differences
 621 less than 5%, in the middle stratosphere, except for OMPS LP in the northern mid-latitudes near

622 28–31 km (Figures 10c, 11). This is due to the thermal sensitivity problem in the OMPS LP
 623 instrument, which causes negative biases of 10–15% in retrieved ozone from the visible spectral
 624 ranges (Kramarova et al., 2018). In the upper stratosphere and lower mesosphere (e.g., above
 625 ~45 km) the differences between SAGE III and other correlative measurements become larger.
 626 This is due to the ozone diurnal cycle and/or known biases in those datasets. For example, SAGE
 627 III shows negative biases of 5–10% relative to ACE-FTS in the upper stratosphere and lower
 628 mesosphere. This is due to known positive biases in ACE-FTS ozone in those regions (Sheese et
 629 al., 2017). SAGE III also shows altitude dependent high biases versus OMPS LP, with mean
 630 differences of ~5% at 45 km and ~15–20% at 52 km (Figure 11). This is an artifact resulting
 631 from the known low biases (~10%) in OMPS LP ozone in the upper stratosphere and lower
 632 mesosphere (Kramarova et al., 2018) and the ozone diurnal cycle. In the upper stratosphere and
 633 mesosphere, the ozone levels show a strong depletion during the daytime and recover at night.
 634 The OMPS LP measurements mainly occurs during daytime (e.g., at local solar time ~1:30 PM),
 635 while SAGE III takes measurements during sunrise and sunset when ozone values are closer to
 636 nighttime measurements. The day-night ozone differences are ~10% at 50 km and increase to
 637 ~60% at 65 km (Parish et al., 2014). The low biases in OMPS LP ozone for altitudes above 45
 638 km, therefore, would be further enhanced by the ozone diurnal cycle when compared with SAGE
 639 III, and result in altitude-dependent structure as shown in Figure 11.



640

641 **Figure 11:** Mean differences (top) and standard deviations (bottom) between SAGE III/ISS AO3
 642 against Aura MLS (red), ACE-FTS (blue), OSIRIS (green), and OMPS LP (pink) in three wide
 643 latitude bands.

644 The comparisons between SAGE III and OSIRIS ozone for altitudes above ~50 km show
 645 similar features (e.g., altitude-dependent biases) as those in SAGE III/OMPS LP comparisons.
 646 OSIRIS is on a sun synchronous satellite, which observes ozone mainly at local solar time
 647 between 6:30 and 7:30 am (closer to daytime ozone values). The observed differences between

648 SAGE III and OSIRIS for altitudes above 50 km are consistent with what we expect from day-
649 night ozone differences. The effects of the ozone diurnal cycle on the comparisons between
650 SAGE III and Aura MLS or ACE-FTS in the upper stratosphere and lower mesosphere are
651 smaller. This is because MLS nighttime measurements (~1:45 am) were used in this study, and
652 the ACE-FTS also makes measurements during local sunrise or sunset.

653 In the lower stratosphere and upper troposphere SAGE III ozone in general shows high
654 biases against other correlative satellite measurements, with mean relative differences of ~5–
655 10% against Aura MLS and ACE-FTS from 20 km down to the tropopause. Most, if not all, of
656 this bias is likely the result of the O₄ spectroscopy problem discussed in section 2.2. The
657 differences between SAGE III and OSIRIS and OMPS LP are larger (~10–20%) in the southern
658 hemisphere mid-latitudes and in the tropics. This is most likely related to low biases in OSIRIS
659 and OMPS LP ozone measurements in the UT/LS regions (Kramarova et al., 2018; Adams et al.,
660 2014).

661 The standard deviations of relative differences between SAGE III and other satellite
662 measurements, except ACE-FTS, show similar magnitudes and vertical structures. The smallest
663 standard deviations of ~5% are found in the middle stratosphere (e.g., between 20 and 40 km).
664 The standard deviations increase to ~10% at 50 km and ~20% at 60 km. The smaller standard
665 deviations between SAGE III and ACE-FTS differences in the upper stratosphere and lower
666 mesosphere are due to both instruments making observations during sunrise and sunset with
667 smaller noise. Below 20 km the standard deviations also become larger. These increases result
668 from both measurement uncertainties and mismatch (inexact coincidence) between SAGE III and
669 other satellites. The lower stratosphere and upper troposphere is a challenging area for satellite
670 ozone observations. SAGE III ozone in the UT/LS will be further evaluated by ground-based
671 measurements in the following section.

672 5.3 Comparisons between SAGE III/ISS and ground-based measurements

673 The ozonesondes and stratospheric ozone lidars were used to further evaluate the SAGE
674 III/ISS ozone in the UT/LS region. The geolocations and data sources of ozonesondes and lidar
675 and number of coincident profiles found for each with SAGE III are listed in Table 1 and Table
676 2, respectively. For ozonesondes the tropical stations are mainly from the Southern Hemisphere
677 ADditional OZonesondes (SHADOZ) network (Thompson et al., 2017; Witte et al., 2017).
678 Although there are few coincident profiles (e.g., from 1 to 8) between SAGE III and individual
679 ozonesonde stations in SHADOZ, the ozonesondes data have been processed with the same
680 processing technique to minimize the inhomogeneities in ozonesonde data records. This enables
681 us to group SHADOZ data in the tropics to provide better statistics for estimating SAGE III
682 ozone biases in that region. Outside the tropical latitudes, ozonesondes from the WOUDC and
683 NOAA Earth System Research Laboratory (ESRL) (Johnson et al., 2018) were used. There are
684 five NDACC stratospheric ozone lidar stations that provide correlative measurements during the
685 first two years of SAGE III operation (e.g., June 2017 to May 2019). Those stations are listed in
686 Table 2.

687

688

689

690 **Table 1** ozonesonde stations used in this study

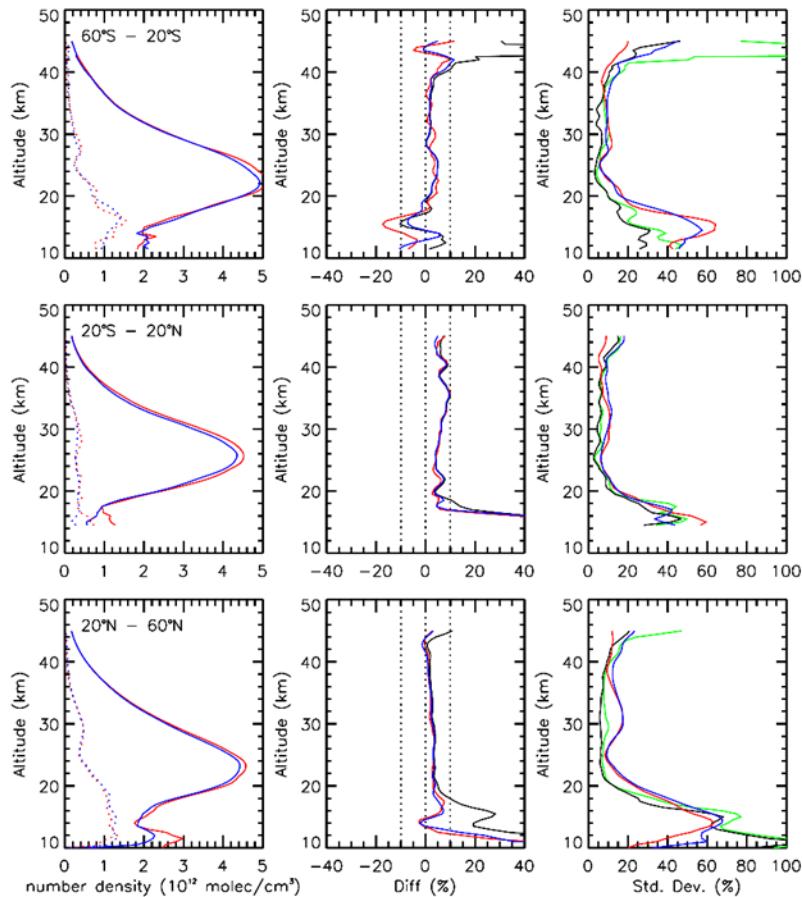
Station	Latitude	Longitude	Data source	Coincident profiles
Hohenpeissenberg	47.80	11.00	WOUDC	53
Payerne	46.49	6.57	WOUDC	56
Trinidad Head	41.06	-124.15	NOAA	13
Boulder	39.95	-105.20	NOAA	21
Tsukuba	36.06	140.13	WOUDC	17
Huntsville	34.73	-86.85	NOAA	8
Hilo	19.40	-155.40	SHADOZ/NOAA	8
Costa Rica	9.94	-84.04	SHADOZ	5
Paramaribo	5.80	-55.20	SHADOZ	1
Kuala Lumpur	2.73	101.70	SHADOZ	7
Nairobi	-1.30	36.80	SHADOZ	6
Natal	-5.40	-35.40	SHADOZ	3
Ascension Is.	-7.56	-14.22	SHADOZ	5
Am. Samoa	-14.20	-170.60	SHADOZ/NOAA	3
Fiji	-18.10	178.40	SHADOZ	5
La Reunion Is.	-21.10	55.50	SHADOZ	1
Irene	-25.90	28.20	SHADOZ	4
Broadmeadows	-37.69	144.95	WOUDC	13
Lauder	-45.04	169.68	WOUDC	29
Macquarie Is.	-54.50	158.94	WOUDC	13

691

692 **Table 2** Lidar data used in this study

Station	Latitude	Longitude	Data source	Coincident profiles
Hohenpeissenberg	47.80	11.00	NDACC	38
OHP	43.92	5.71	NDACC	46
Table Mtn.	34.5	-117.7	NDACC	45
Mauna Loa	19.47	-155.60	NDACC	30
Lauder	-45.04	169.68	NDACC	13

693 Due to limited coincident profiles between SAGE III and ground-based measurements
694 the medians and spreads (defined as one-half of the differences between the 84th and 16th
695 percentiles) of relative differences are better diagnostics to represent the biases and random
696 errors in SAGE III retrieved ozone. The median and spread are the same as the mean and
697 standard deviation when the statistical sample has a Gaussian distribution (e.g., Wang et al.,
698 2002). The occurrence of outliers in the distribution, however, can lead to larger standard
699 deviations and introduce a discrepancy between the mean and median for a non-Gaussian
700 (asymmetric) distribution. For comparisons between SAGE III (or other satellites) and ground-
701 based measurements, there could be outliers in the statistical sample due to anomalous data not
702 being filtered out and/or large dynamic variability in the UT/LS (i.e., mismatch between SAGE
703 III and ground-based measurements). The median and spread are more robust statistics to
704 minimize the effect of outliers, especially for a distribution with small sample size.

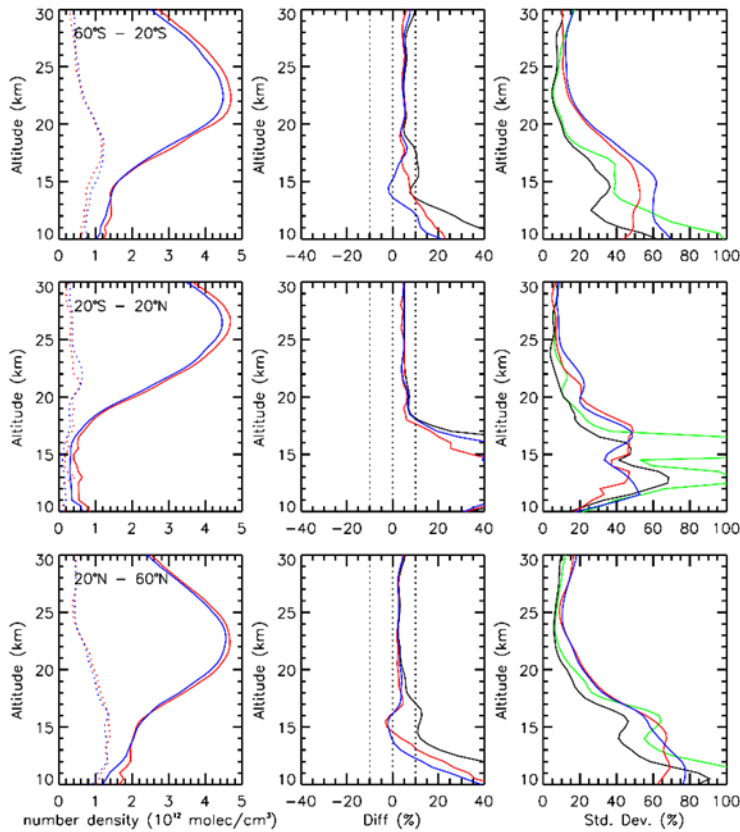


705

706 **Figure 12:** Comparisons between SAGE III/ISS and correlative lidar at three latitude bands,
 707 60°S–20°S (top panel), 20°S–20°N (middle panel) and 20°N–60°N (bottom panel). The mean
 708 (solid lines) and standard deviation (dotted lines) of coincident SAGE III/ISS (red) and lidar
 709 (blue) ozone number density profiles are shown in the left panel. The relative percentage
 710 differences between SAGE III/ISS and lidar are shown in the middle panel. The mean and
 711 median of relative differences are indicated by the black and red colors, respectively. The blue
 712 lines indicates differences estimated from averaged ozone profiles (see text). In the right panel,
 713 the standard deviations of mean and 1- σ spreads of median differences are indicated by green
 714 and black lines, respectively. The standard deviations of coincident SAGE III/ISS (red) and lidar
 715 (blue) profiles are also shown.

716 The comparison results between SAGE III and lidar are shown in Figure 12. The analysis
 717 is performed by using all collocated profiles in three broad latitude bands, southern mid-latitudes
 718 (60°S–20°S), tropics (20°S–20°N), and northern mid-latitudes (20° N–60°N). There is only one
 719 lidar station, Lauder and Mauna Loa, located in the southern mid-latitude and tropics,
 720 respectively. For northern mid-latitudes, measurements from Hohenpeissenberg, Observatoire de
 721 Haute-Provence (OHP), and Table Mountain Facility are used. Both SAGE III and lidar show
 722 maximum ozone concentrations near 22–23 km in the mid-latitudes and 26–27 km in the tropics
 723 (Figure 12 left panel). The ozone variabilities indicated by the standard deviations generally
 724 increase from the upper stratosphere down to the lower stratosphere and upper troposphere.
 725 SAGE III and lidar observations show similar results with standard deviations between 10–20%

726 for altitudes between 20 and 40 km. The standard deviations increase to ~50–60 % in the UT/LS
 727 regions due to larger dynamic variability and smaller ozone amounts (Figure 12 right panel). The
 728 best agreements between SAGE III and lidar are found between 20 and 40 km. SAGE III shows
 729 a small positive bias of ~5% against all lidar observations except at Mauna Loa, where SAGE III
 730 ozone shows slightly larger high biases of ~5–10% between 30 and 40 km (Figure 12 middle
 731 panel). The reason for this is not clear, but SAGE III ozone is in good agreement (within 5%)
 732 with other satellites at the same altitude ranges in the tropics (Figure 11).



733

734 **Figure 13:** Similar to figure 12 but for comparisons between SAGE III/ISS and ozonesondes.

735 In the southern mid-latitudes above ~42 km, SAGE III and Lauder ozone lidar show
 736 mean differences of ~40% or larger and standard deviations greater than 60%. The median
 737 differences, however, are only $\pm 10\%$. The larger mean differences and standard deviations,
 738 compared to medians and spreads, between SAGE III and Lauder in the upper stratosphere are
 739 due to outliers in the lidar measurements. Those outliers also contribute to larger standard
 740 deviations (by approximately a factor of 2 than SAGE III) in lidar observed ozone values (Figure
 741 12 right panel).

742 In the lower stratosphere below 20 km, the systematic (median) differences between
 743 SAGE III and lidar measurements are within 10% except for Lauder. The systematic biases
 744 between SAGE III and lidar can be approximated (to first order) by the relative difference
 745 between averaged SAGE III and lidar ozone values (e.g., $(\bar{S} - \bar{L})/\bar{L}$, where \bar{S} and \bar{L} indicate
 746 averaged ozone values from all collocated SAGE III and lidar profiles, respectively). This

747 method can also minimize the sensitivity of outliers. It yields similar results as those from the
 748 median of relative differences, except in the lower stratosphere at Lauder (Figure 12 middle
 749 panel). This is probably related to the fact that samples of coincident SAGE III and lidar ozone
 750 profiles at Lauder are too small (i.e., 13 profiles).

751 Similar analyses were performed between SAGE III and ozonesondes and the results are
 752 shown in Figure 13. In the mid-latitudes, SAGE III ozone values are generally biased high
 753 against ozonesondes with differences of ~5% for altitudes above 15 km. The biases increase
 754 toward the lower stratosphere and upper troposphere, and reach ~10% at 12–13km. The standard
 755 deviations (approximated by the spreads) of mean relative differences are ~5% near the ozone
 756 peak and become larger at higher and lower altitudes. The standard deviations increase to ~30–
 757 40% at 15 km and ~50% near the tropopause. The comparisons between SAGE III and
 758 ozonesondes in the tropics show similar vertical structure as those in the mid-latitudes. SAGE III
 759 ozone values are systematically higher than sonde ozone values by ~5% for altitudes above 20
 760 km. The biases increase rapidly toward the UT/LS, and reaches ~10% at 17–18 km and ~40% (or
 761 higher) at 15–16 km. It should be noted that comparison results for altitudes below 17 km in the
 762 tropics are not robust because both the standard deviations and spreads of relative differences are
 763 larger than those of SAGE III and ozonesondes measurements and combined uncertainties
 764 (Figure 13). Similar situations also occurs for altitudes below 12 km in the mid-latitudes.

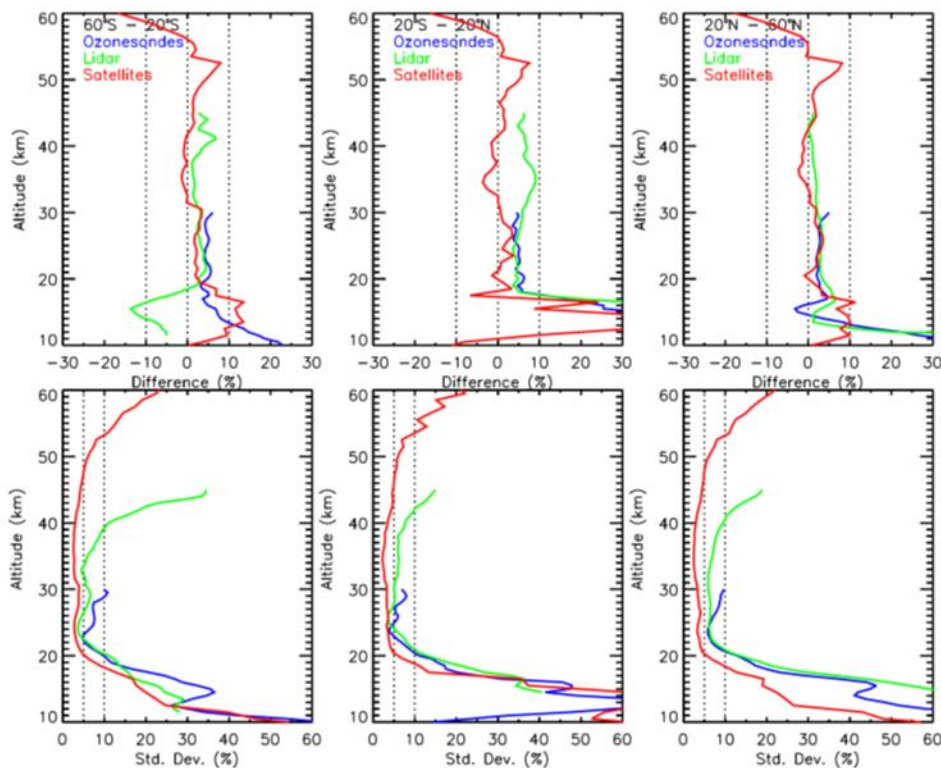
765 5.4 Estimated accuracies and precisions of SAGE III/ISS AO3 ozone

766 The comparisons between SAGE III/ISS solar ozone data and correlative satellite and
 767 ground-based measurements are summarized in Figure 14. Since there is known thermal
 768 sensitivity issue in the OMPS LP ozone data (Kramarova et al., 2018), the OMPS LP data
 769 between 28 and 32 km (e.g., Figure 11) were filtered before calculating the means and standard
 770 deviations of relative differences between SAGE III and other satellites. There is no additional
 771 filtering for Aura MLS, ACE-FTS, OSIRIS, lidar and ozonesonde data. The median and spread
 772 are used for comparisons between SAGE III and ground based measurements for reasons
 773 discussed earlier. Based on these correlative measurements, the accuracy of SAGE III/ISS AO3
 774 ozone in the stratosphere is better than 5% for altitudes down to 15 km in the mid-latitudes and
 775 20 km in the tropics. The accuracy degrades toward lower altitudes and reaches ~10% at the
 776 tropopause. In the southern hemisphere mid-latitudes the SAGE III/ISS ozone show larger than
 777 10% positive bias near 15 km comparing to correlative satellite data (Figure 14). This is due to
 778 larger biases between SAGE III/ISS and OMPS LP and OSIRIS in that region (e.g., Figure 11).
 779 The SAGE III/ISS, however, shows much better agreement (<10%) with Aura MLS and
 780 ozonesondes in the same region. The larger biases (>5%) between SAGE III/ISS and other
 781 satellites for altitudes above ~50 km is due to the diurnal cycle effects not being removed from
 782 the comparisons which has been discussed earlier in section 5.2.

783 The standard deviation of relative differences between SAGE III/ISS and correlative
 784 measurements can be used as an approximation of measurement uncertainty in the SAGE III
 785 instrument. It, however, becomes invalid when the uncertainties (random error) of correlative
 786 measurements become larger and/or the uncertainties due to temporal/spatial differences are
 787 large. The variance of the differences between SAGE III and collocated measurements contains
 788 uncertainties from not only SAGE but also correlative measurements and from uncertainties
 789 associated with natural variability (e.g., Sofieva et al., 2014).

$$\sigma^2(x_s - x_c) = \sigma^2(x_s) + \sigma^2(x_c) + \sigma^2(nat)$$

790 where x_s and x_c are SAGE III and correlative measurements, respectively. The $\sigma^2(nat)$ is the
 791 variance contributed by the natural variability, which can be minimized by using coincident
 792 criteria. The uncertainties of satellite measurements generally become larger toward the UT/LS
 793 regions. This can be seen in Figure 14, where the standard deviations of relative differences
 794 between SAGE III and correlative satellite measurements increase from ~5% at 20 km to ~50–
 795 60% near 10 km. Although the ground-based measurements (e.g., ozonesondes) have better
 796 precisions in the UT/LS region, the mismatch errors between SAGE III and ground-based
 797 measurements are larger (e.g., due to larger coincident criteria). Furthermore, the satellite
 798 measurements cover a larger air mass while ground-based observations represent a much smaller
 799 area. The different horizontal resolution (e.g., smoothing error) could further enhance the
 800 mismatch error. Due to the above-mentioned reasons, the standard deviations between SAGE III
 801 and ground-based measurements are similar or even larger than those in SAGE III and satellite
 802 comparisons (Figure 14).

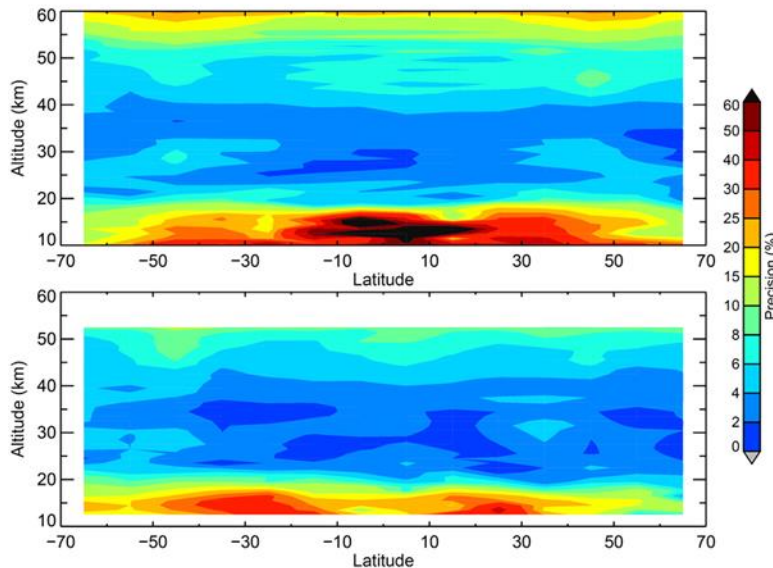


803

804 **Figure 14:** Mean (or median) differences (top panel), and the standard deviations (or spreads) of
 805 differences (bottom panel) between SAGE III-ISS ozone and coincident measurements from
 806 satellites (red line), lidar (green line) and ozonesondes (blue line) at three latitude bands, 60°S–
 807 20°S (left column), 20°S–20°N (middle column) and 20°N–60°N (right column). Results
 808 between SAGE III and ground based measurements (lidar and ozonesondes) are based on
 809 medians and spreads, while comparisons between SAGE III and other satellites are based on
 810 mean and standard deviation.

811 To better assess the precisions of SAGE III ozone measurements especially in the UT/LS,
 812 we used the method in Fioletov et al. (2006). In Fioletov et al. (2006), it is assumed that paired
 813 measurements are perfectly collocated (i.e., no mismatch error). In reality it is almost impossible

814 to have SAGE III and correlative measurements at the same location and time. The effect of
 815 spatial and temporal differences, however, could be minimized by using tighter coincident
 816 criteria. We used smaller coincident criteria of latitude differences within $\pm 1^\circ$, longitude
 817 differences within $\pm 5^\circ$, and the closest in time within the same day for this purpose. The
 818 estimated precisions of SAGE III AO3 ozone based on comparisons with correlative Aura MLS
 819 and OMPS LP data are shown in Figure 15. We did not use other correlative satellite or ground-
 820 based measurements because there were fewer coincident profiles with SAGE III compared to
 821 those with Aura MLS and OMPS LP.



822

823 **Figure 15:** Estimated precisions in SAGE III/ISS AO3 ozone based on comparisons with
 824 collocated Aura MLS (top) and OMPS LP (bottom) data between June 2017 and May 2019.

825 By comparing SAGE III/ISS against collocated Aura MLS measurements the estimated
 826 precision of SAGE III ozone is approximately 3% (e.g., 2–4%) between 20 and 40 km, and ~10–
 827 15% at 55 km (Figure 15). Below 20 km, the precisions of SAGE III ozone degrade toward
 828 lower altitudes and reach ~20–30% near the tropopause. Similar results can be seen in the
 829 comparisons between SAGE III and OMPS LP except in the tropical UT/LS region. Since both
 830 analyses, between SAGE III and Aura MLS and OMPS LP, show consistent results, this
 831 indicates that the derived precisions of SAGE III ozone data are robust. The estimated precisions
 832 of SAGE III ozone shown in Figure 15 are in general slightly larger than the random errors
 833 reported by the SAGE retrieval algorithm (e.g., Figure 4). This is probably due to the small
 834 residual effect of spatial and temporal differences between SAGE III and correlative
 835 measurements (mismatch error cannot be completely removed from the analyses by the
 836 coincident criteria).

837 6 Conclusions

838 The Stratospheric Aerosol and Gas Experiment III on the International Space Station
 839 (SAGE III/ISS) was launched in February 2017 and started routine operation in June 2017. It is
 840 the second SAGE III instrument but with better latitudinal coverage. Similar to SAGE II, it
 841 provides near global observations on a monthly basis. The first two years of SAGE III/ISS

842 version 5.1 solar ozone data were evaluated by using correlative measurements from satellites
843 (Aura MLS, ACE-FTS, OSIRIS, OMPS LP) and ground-based instruments (lidar and
844 ozonesondes). There are three retrieved ozone products, denoted as AO3, MLR, and MES, from
845 SAGE III solar occultation measurements. The first two (AO3 and MLR) algorithms both use
846 ozone absorption in the Chappuis band but different methods to separate ozone and other
847 interfering gases from the observed slant path radiances (SAGE III ATBD, 2002). The third
848 algorithm (MES) uses ozone absorption in the ultraviolet band, which can provide better ozone
849 signals at higher altitudes (e.g., above 45 km). The MES retrieval algorithm, however, is affected
850 by a spectral stray light problem, which has not been properly corrected. The MES ozone
851 product, therefore, is currently not recommended for scientific studies.

852 To evaluate the quality of SAGE III/ISS solar ozone data, appropriate procedures have
853 been applied to SAGE III and correlative measurements to minimize the biases and uncertainties
854 associated with mismatch (spatial/temporal differences) and different smoothing (e.g.,
855 resolutions) in respective observations. The coincident criteria are a trade-off between mismatch
856 uncertainties and large sample size (number of coincident profiles), especially for comparisons
857 between SAGE III and ground-based measurements. There is no good way to remove the
858 horizontal component of smoothing differences, which, however, would be reflected as random
859 errors in statistics with a sufficiently large sample size (e.g., Cortesi et al., 2007). The method
860 recommended by the instrument science team or Gaussian kernel (e.g., Kar et al., 2007; Sheese
861 et al., 2017) was applied to the profiles with finer vertical resolution to remove/minimize the
862 vertical component of smoothing differences. Since there are altitude registration errors of
863 approximately 100 m in the auxiliary temperature and pressure profiles in SAGE III/ISS version
864 5.1 data, we used ozone number density on geometric altitude as the common coordinate for
865 comparisons. The altitude registration errors in SAGE III temperature and pressure profiles are
866 due to a simplistic approximation in the geopotential height to geometric altitude conversion. It
867 should be noted that this error would not affect SAGE III ozone on its native retrieved grids,
868 number density and geometric altitude, unless the profiles are converted to mixing ratio on
869 pressure coordinate by using the auxiliary temperature and pressure profile accompanying each
870 ozone profile.

871 For ozone retrieved from the AO3 and MLR algorithm, it was found that MLR ozone has
872 larger biases (e.g., by 10% or higher) and uncertainties (by a factor of 2 to 3) in the UT/LS and
873 above the upper stratosphere by comparisons with correlative measurements or using residual
874 analyses (Damadeo et al., 2014). These results are similar to a previous study (Wang et al., 2006)
875 for the SAGE III/M3M instrument. SAGE III/ISS AO3 ozone show very good agreement with
876 correlative measurements, with mean biases less than 5% for altitudes down to ~15 km in the
877 mid-latitudes and ~20 km in the tropics. The differences become larger in the lower mesosphere
878 (e.g., 10–15% near 60 km), which mainly results from the ozone diurnal cycle not being
879 removed from the comparisons. In the lower stratosphere and upper troposphere, the SAGE
880 III/ISS AO3 ozone show systematic high biases that increase with decreasing altitudes, and reach
881 ~10% near the tropopause. The precision of SAGE III/ISS AO3 ozone is estimated to be ~3%
882 between 20 and 40 km. The precisions degrades toward higher and lower altitudes due to smaller
883 signal to noise ratio in Chappuis band and large natural variability in the UT/LS region. The
884 estimated precision in AO3 ozone is ~10–15% in the lower mesosphere (55 km), and ~20–30%
885 near the tropopause.

886 The sunrise/sunset differences in SAGE III/ISS retrieved ozone were examined by
 887 regression analyses and comparisons with correlative Aura MLS data. It was found that SAGE
 888 III sunset ozone values are systematically larger than sunrise values by ~5–8%, at 40–55 km with
 889 mean differences larger in the tropics than at mid-latitudes. In the lower stratosphere below ~25
 890 km, the sunrise values become slightly larger than sunset values by a few percent. The vertical
 891 and latitudinal distribution of sunrise/sunset differences in observed ozone is consistent with the
 892 vertical transport of atmospheric tidal winds (Sakazaki et al., 2013). The magnitude of
 893 sunrise/sunset differences in SAGE III/ISS retrieved ozone in the upper stratosphere, however,
 894 are almost twice as large as those observed from other satellites and model prediction (Sakazaki
 895 et al., 2015). The reason for this is not clear and needs further investigation. The SAGE III
 896 retrieval algorithm team is investigating the high biases in retrieved ozone in the UT/LS region.
 897 Preliminary studies indicate that the oxygen dimer O₂-O₂ (or O₄) spectroscopy used in the
 898 current v5.1 retrieval algorithm could primarily contribute to the observed high biases in ozone.
 899 It was also found that an under estimation of aerosol contribution in the ozone absorption band
 900 could indicate a potentially small high bias in stratospheric ozone in both the AO3 and MLR
 901 algorithms. The effects are more pronounced in the MLR than the AO3 algorithm. This is
 902 consistent with our validation results, which show altitude-dependent high biases in both MLR
 903 and AO3 retrieved ozone for altitudes below 15–20 km. The biases in MLR ozone are also larger
 904 than those in AO3. Further analyses will be made in the future by applying updated O₄
 905 spectroscopy and aerosol clearing procedures in the retrieval algorithm to quantify these effects
 906 on retrieved ozone in the upper troposphere and lower stratosphere.

907 Appendix

908 As a known anomaly in v5.1, Section 2.2 describes an altitude registration bias in the
 909 reported pressure and temperature profiles that are passed through the algorithm. This Appendix
 910 details a recommended conversion from which Figure 2 derives. The process involves three
 911 simple steps: 1) convert the geometric altitude array upon which the pressures and temperatures
 912 are reported (Z_{OLD}) back to the original geopotential heights (Z_{Φ}) using the approximation used
 913 in the v5.1 algorithm, 2) convert the geopotential heights to geometric altitude (Z_{NEW}) using a
 914 better model, and 3) remap the reported pressures and temperatures on the new geometric
 915 altitudes to the desired grid (such as the original grid) using your favorite interpolation scheme.
 916 Step 1 is very straightforward, and comes from the overly simplistic assumption that the surface
 917 gravity is the same everywhere and is equal to the mean surface gravity (g_0) defined as 9.80665
 918 m/s²):

$$Z_{\Phi} = \frac{Z_{OLD} * R_{EARTH}}{R_{EARTH} + Z_{OLD}}$$

919 Step 2 is also straightforward:

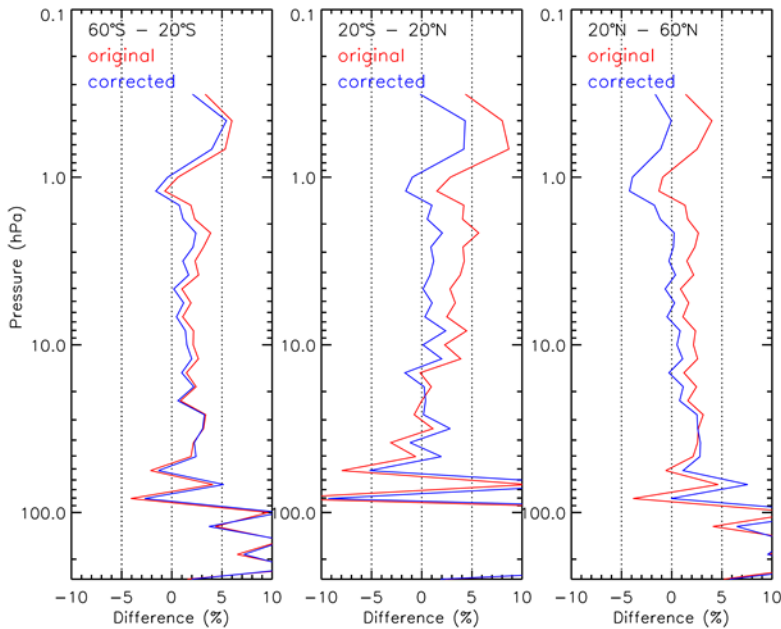
$$Z_{NEW} = \frac{Z_{\Phi} * R_{EARTH}}{\frac{g(\theta)}{g_0} * R_{EARTH} - Z_{\Phi}}$$

920 where g is the surface gravity at a particular geodetic latitude (θ , or “map” latitude).
 921 While the model of surface gravity is always being updated, the SAGE algorithm makes use of
 922 the World Geodetic System 1984 model (WGS84, updated in 2004) (NIMA Technical Report,
 923 1997) and thus this provides the recommendation for g :

$$g(\theta) = 9.7803253359 \frac{1 + 0.00193185265241 * \text{SIN}^2(\theta)}{\sqrt{1 - 0.00669437999013 * \text{SIN}^2(\theta)}}$$

924 It is important to note that the latitude-dependence of R_{EARTH} should be taken into account for all
 925 of these calculations.

926



927

928 **Figure S1:** Mean differences between SAGE III/ISS AO3 ozone and collocated Aura MLS data
 929 at three latitude bands 60°S–20°S (left column), 20°S–20°N (middle column), and 20°N–60°N
 930 (right column). SAGE ozone profiles are converted to MLS coordinates by using reported (red)
 931 and bias corrected (blue) temperature and pressure profiles. The percentage difference is
 932 calculated as $(\text{SAGE-MLS})/\text{MLS} * 100\%$.

933 To evaluate the effect of altitude registration bias in the reported temperature and
 934 pressure profiles on ozone, SAGE III/ISS AO3 ozone data were compared against collocated
 935 Aura MLS nighttime measurements on volume mixing ratio and pressure coordinates (VMR/P).
 936 The coincidence criteria are the same as those described in section 4. SAGE III/ISS AO3 ozone
 937 profiles were converted to VMR/P by using accompanying temperature and pressure profiles.
 938 The mean biases between SAGE and MLS are generally within 5% between ~83 and 0.3 hPa
 939 except in the tropics, where larger biases (>5%) are found below ~46 and above 1 hPa (Figure
 940 S1). It should be noted that the differences between SAGE and MLS in the tropics show an
 941 altitude-dependent structure. SAGE ozone shows increasing positive biases for altitudes above
 942 the ozone peak while increasing negative biases below the ozone peak. This is due to the altitude
 943 registration errors in reported temperature and pressure profiles that are more pronounced in the
 944 tropics than mid-latitudes (Figure 2). After correcting the altitude registration errors in the
 945 reported temperature and pressure profiles the SAGE ozones show better agreement with MLS
 946 data without the altitude-dependent feature. The mean differences in general are less than 3% for

947 altitudes between 1 and ~83 hPa in the mid-latitudes and between 1 and ~56 hPa in the tropics
 948 (Figure S1).

949 **Acknowledgments**

950 The authors would like to thank Bryan Johnson at Earth System Research Laboratory, Global
 951 Monitoring Division, NOAA for some ozonesonde data in NOAA's network. The lidar data used
 952 in this publication were obtained from the Network for the Detection of Atmospheric
 953 Composition Change (NDACC) and are publicly available (see <http://www.ndacc.org>). We also
 954 want to thank WMO/GAW Ozone Monitoring Community, World Meteorological Organization-
 955 Global Atmosphere Watch Program (WMO-GAW)/World Ozone and Ultraviolet Radiation Data
 956 Centre (WOUDC) for ozonesonde data. Retrieved May 2019 from <https://woudc.org>. A list of all
 957 contributors is available on the website. doi:10.14287/10000008. This work was funded by the
 958 National Aeronautics and Space Administration (NASA) on Grant Number 80NSSC18K0710.
 959 The Atmospheric Chemistry Experiment (ACE) is a Canadian-led mission mainly supported by
 960 the Canadian Space Agency.

961 **References**

- 962 Adams, C., Bourassa, A. E., Bathgate, A. F., McLinden, C. A., Lloyd, N. D., Roth, C. Z.,
 963 Llewellyn, E. J., Zawodny, J. M., Flittner, D.E., Manney, G.L., Daffer, W.H., and
 964 Degenstein, D.A.: Characterization of Odin-OSIRIS ozone profiles with the SAGE II
 965 dataset, *Atmos. Meas. Tech.*, 6, 1447–1459, doi:10.5194/amt6-1447-2013, 2013.
- 966 Adams, C., Bourassa, A. E., Sofieva, V., Froidevaux, L., McLinden, C. A., Hubert, D., Lambert,
 967 J.-C., Sioris, C. E., and Degenstein, D. A.: Assessment of Odin-OSIRIS ozone
 968 measurements from 2001 to the present using MLS, GOMOS, and ozonesondes, *Atmos.*
 969 *Meas. Tech.*, 7, 49-64, <https://doi.org/10.5194/amt-7-49-2014>, 2014.
- 970 Bernath, P. F., McElroy, C. T., Abrams, M. C., Boone, C. D., Butler, M., Camy-Peyret, C.,
 971 Carleer, M., Clerbaux, C., Coheur, P.-F., Colin, R., DeCola, P., DeMazière, M.,
 972 Drummond, J. R., Dufour, D., Evans, W. F. J., Fast, H., Fussen, D., Gilbert, K., Jennings,
 973 D. E., Llewellyn, E. J., Lowe, R. P., Mahieu, E., McConnell, J. C., McHugh, M.,
 974 McLeod, S. D., Michaud, R., Midwinter, C., Nassar, R., Nichitiu, F., Nowlan, C.,
 975 Rinsland, C. P., Rochon, Y. J., Rowlands, N., Semeniuk, K., Simon, P., Skelton, R.,
 976 Sloan, J. J., Soucy, M.-A., Strong, K., Tremblay, P., Turnbull, D., Walker, K. A., Walkty,
 977 I., Wardle, D. A., Wehrle, V., Zander, R., and Zou, J.: Atmospheric Chemistry
 978 Experiment (ACE): Mission overview, *Geophys. Res. Lett.*, 32, L15S01,
 979 doi:10.1029/2005GL022386, 2005.
- 980 Boone, C. D., Nassar, R., Walker, K. A., Rochon, Y., McLeod, S. D., Rinsland, C. P., and
 981 Bernath, P. F.: Retrievals for the Atmospheric Chemistry Experiment Fourier-transform
 982 spectrometer, *Appl. Optics*, 44(33), 7218–7231, 2005.
- 983 Boone, C. D., Walker, K. A., and Bernath, P. F.: Version 3 Retrievals for the Atmospheric
 984 Chemistry Experiment Fourier Transform Spectrometer (ACE-FTS), The Atmospheric
 985 Chemistry Experiment ACE at 10: A Solar Occultation Anthology, A. Deepak
 986 Publishing, Hampton, Virginia, USA, 103–127, 2013.

- 987 Bourassa, A. E., Degenstein, D. A., and Llewellyn, E. J.: SASKTRAN: A spherical geometry
 988 radiative transfer code for efficient estimation of limb scattered sunlight, *J. Quant.*
 989 *Spectrosc. Ra.*, 109, 52–73, doi:10.1016/j.jqsrt.2007.07.007, 2008.
- 990 Bourassa, A. E., Roth, C. Z., Zawada, D. J., Rieger, L. A., McLinden, C. A., and Degenstein, D.
 991 A.: Drift-corrected Odin-OSIRIS ozone product: algorithm and updated stratospheric
 992 ozone trends, *Atmos. Meas. Tech.*, 11, 489–498, <https://doi.org/10.5194/amt-11-489-2018>,
 993 2018.
- 994 Brühl, C., Drayson, S. R., Russell III, J. M., Crutzen, P. J., McInerney, J. M., Purcell, P. N.,
 995 Claude, H., Gernandt, H., McGee, T. J., McDermid, I. S., and Gunson, M. R.: Halogen
 996 Occultation Experiment ozone channel validation, *J. Geophys. Res.*, 101, 10,217–10,240,
 997 1996.
- 998 Chu, W. P., McCormick, M. P., Lenoble, J., Broniez, C., and Pruvost, P.: SAGE II inversion
 999 algorithm, *J. Geophys. Res.*, 94, 8339–8351, doi:10.1029/JD094iD06p08447, 1989
- 1000 Cortesi, U., Lambert, J. C., De Clercq, C., Bianchini, G., Blumenstock, T., Bracher, A., Castelli,
 1001 E., Catoire, V., Chance, K. V., De Mazière, M., Demoulin, P., Godin-Beekmann, S.,
 1002 Jones, N., Jucks, K., Keim, C., Kerzenmacher, T., Kuellmann, H., Kuttippurath, J.,
 1003 Iarlori, M., Liu, G. Y., Liu, Y., McDermid, I. S., Meijer, Y. J., Mencaraglia, F., Mikuteit,
 1004 S., Oelhaf, H., Piccolo, C., Pirre, M., Raspollini, P., Ravegnani, F., Reburn, W. J.,
 1005 Redaelli, G., Remedios, J. J., Sembhi, H., Smale, D., Steck, T., Taddei, A., Varotsos, C.,
 1006 Vigouroux, C., Waterfall, A., Wetzell, G., and Wood, S.: Geophysical validation of
 1007 MIPAS-ENVISAT operational ozone data, *Atmos. Chem. Phys.*, 7, 4807–4867,
 1008 <https://doi.org/10.5194/acp-7-4807-2007>, 2007.
- 1009 Damadeo, R. P., Zawodny, J. M., Thomason, L. W., and Iyer, N.: SAGE version 7.0 algorithm:
 1010 application to SAGE II, *Atmos. Meas. Tech.*, 6, 3539–3561, [https://doi.org/10.5194/amt-](https://doi.org/10.5194/amt-6-3539-2013)
 1011 [6-3539-2013](https://doi.org/10.5194/amt-6-3539-2013), 2013
- 1012 Damadeo, R. P., Zawodny, J. M., and Thomason, L. W.: Reevaluation of stratospheric ozone
 1013 trends from SAGE II data using a simultaneous temporal and spatial analysis, *Atmos.*
 1014 *Chem. Phys.*, 14, 13455–13470, <https://doi.org/10.5194/acp-14-13455-2014>, 2014.
- 1015 Damadeo, R., Zawodny, J. M., Remsberg, E. E., and Walker, K. A.: The impact of nonuniform
 1016 sampling on stratospheric ozone trends derived from occultation instruments, *Atmos.*
 1017 *Chem. Phys.*, 18, 535–554, <https://doi.org/10.5194/acp-18-535-2018>, 2018.
- 1018 Degenstein, D. A., Bourassa, A. E., Roth, C. Z., and Llewellyn, E. J.: Limb scatter ozone
 1019 retrieval from 10 to 60 km using a multiplicative algebraic reconstruction technique,
 1020 *Atmos. Chem. Phys.*, 9, 6521–6529, doi:10.5194/acp-9-6521-2009, 2009.
- 1021 Dupuy, E., Walker, K. A., Kar, J., Boone, C. D., McElroy, C. T., Bernath, P. F., Drummond, J.
 1022 R., Skelton, R., McLeod, S. D., Hughes, R. C., Nowlan, C. R., Dufour, D. G., Zou, J.,
 1023 Nichituiu, F., Strong, K., Baron, P., Bevilacqua, R. M., Blumenstock, T., Bodeker, G. E.,
 1024 Borsdorff, T., Bourassa, A. E., Bovensmann, H., Boyd, I. S., Bracher, A., Brogniez, C.,
 1025 Burrows, J. P., Catoire, V., Ceccherini, S., Chabrilat, S., Christensen, T., Coffey, M. T.,
 1026 Cortesi, U., Davies, J., De Clercq, C., Degenstein, D. A., De Mazière, M., Demoulin, P.,
 1027 Dodion, J., Firanski, B., Fischer, H., Forbes, G., Froidevaux, L., Fussen, D., Gerard, P.,
 1028 GodinBeekmann, S., Goutail, F., Granville, J., Griffith, D., Haley, C. S., Hannigan, J. W.,
 1029 Höpfner, M., Jin, J. J., Jones, A., Jones, N. B., Jucks, K., Kagawa, A., Kasai, Y.,

- 1030 Kerzenmacher, T. E., Kleinböhl, A., Klekociuk, A. R., Kramer, I., Küllmann, H.,
 1031 Kuttippurath, J., Kyrölä, E., Lambert, J.-C., Livesey, N. J., Llewellyn, E. J., Lloyd, N. D.,
 1032 Mahieu, E., Manney, G. L., Marshall, B. T., McConnell, J. C., McCormick, M. P.,
 1033 McDermid, I. S., McHugh, M., McLinden, C. A., Mellqvist, J., Mizutani, K., Murayama,
 1034 Y., Murtagh, D. P., Oelhaf, H., Parrish, A., Petelina, S. V., Piccolo, C., Pommereau, J.-P.,
 1035 Randall, C. E., Robert, C., Roth, C., Schneider, M., Senten, C., Steck, T., Strandberg, A.,
 1036 Strawbridge, K. B., Sussmann, R., Swart, D. P. J., Tarasick, D. W., Taylor, J. R., Tétard,
 1037 C., Thomason, L. W., Thompson, A. M., Tully, M. B., Urban, J., Vanhellemont, F.,
 1038 Vigouroux, C., von Clarmann, T., von der Gathen, P., von Savigny, C., Waters, J. W.,
 1039 Witte, J. C., Wolff, M., and Zawodny, J. M.: Validation of ozone measurements from the
 1040 Atmospheric Chemistry Experiment (ACE), *Atmos. Chem. Phys.*, 9, 287–343,
 1041 doi:10.5194/acp-9-287-2009, 2009.
- 1042 Fioletov, V. E., Tarasick, D. W., and Petropavlovskikh, I.: Estimating ozone variability and
 1043 instrument uncertainties from SBUV(2), ozonesonde, Umkehr, and SAGE II
 1044 measurements: Short-term variations, *J. Geophys. Res.*, 111, D02305,
 1045 doi:10.1029/2005JD006340, 2006.
- 1046 Flittner, D., Bhartia, P. K., and Herman, B. M.: O₃ profiles retrieved from limb scatter
 1047 measurements: Theory, *Geophys. Res. Lett.*, 27, 2601–2604, 2000.
- 1048 Flynn, L. E., Seftor, C. J., Larsen, J. C., and Xu, P.: The Ozone Mapping and Profiler Suite, in:
 1049 Earth Science Satellite Remote Sensing, edited by: Qu, J. J., Gao, W., Kafatos, M.,
 1050 Murphy, R. E., and Salomonson, V. V., Springer, Berlin, 279–296,
 1051 https://doi.org/10.1007/978-3-540-37293-6_15, 2006.
- 1052 Froidevaux, L., Jiang, Y. B., Lambert, A., Livesey, N. J., Read, W. G., Waters, J. W., Browell,
 1053 E. V., Hair, J. W., Avery, M. A., McGee, T. J., Twigg, L. W., Sunnicht, G. K., Jucks, K.
 1054 W., Margitan, J. J., Sen, B., Stachnik, R. A., Toon, G. C., Bernath, P. F., Boone, C. D.,
 1055 Walker, K. A., Filipiak, M. J., Harwood, R. S., Fuller, R. A., Manney, G. L., Schwartz,
 1056 M. J., Daffer, W. H., Drouin, B. J., Cofield, R. E., Cuddy, D. T., Jarnot, R. F., Knosp, B.
 1057 W., Perun, V. S., Snyder, W. V., Stek, P. C., Thurstans, R. P., and Wagner, P. A.:
 1058 Validation of Aura Microwave Limb Sounder stratospheric ozone measurements, *J.*
 1059 *Geophys. Res.*, 113, D15S20, doi:10.1029/2007JD008771, 2008.
- 1060 Gelaro, R., and Coauthors, 2017: The Modern-Era Retrospective Analysis for Research and
 1061 Applications, version 2 (MERRA-2). *J. Climate*, 30, 5419–5454, [https://doi.org/](https://doi.org/10.1175/JCLI-D-16-0758.1)
 1062 [10.1175/JCLI-D-16-0758.1](https://doi.org/10.1175/JCLI-D-16-0758.1).
- 1063 Global Modeling and Assimilation Office (GMAO) (2015), `tavg3_3d_asm_Nv`: MERRA-2 3D
 1064 IAU State, Meteorology time-averaged 3-hourly (model-level, 0.625x0.5L72), version
 1065 5.12.4, Greenbelt, MD, USA: Goddard Space Flight Center Distributed Active Archive
 1066 Center (GSFC DAAC), Accessed May 2019 at doi: 10.5067/SUOQESM06LPK.
- 1067 Godin, S., Carswell, A. I., Donovan, D. P., Claude, H., Steinbrecht, W., McDermid, I. S.,
 1068 McGee, T. J., Gross, M. R., Nakane, H., Swart, D. P. J., Bergwerff, H. B., Uchino, O.,
 1069 von der Gathen, P., and Neuber, R.: Ozone differential absorption lidar algorithm
 1070 intercomparison, *Appl. Opt.*, 38, 6225–6236, doi:10.1364/AO.38.006225, 1999.
- 1071 Hubert, D., Lambert, J.-C., Verhoelst, T., Granville, J., Keppens, A., Baray, J.-L., Bourassa, A.
 1072 E., Cortesi, U., Degenstein, D. A., Froidevaux, L., Godin-Beekmann, S., Hoppel, K. W.,

- 1073 Johnson, B. J., Kyrölä, E., Leblanc, T., Lichtenberg, G., Marchand, M., McElroy, C. T.,
 1074 Murtagh, D., Nakane, H., Portafaix, T., Querel, R., Russell III, J. M., Salvador, J., Smit,
 1075 H. G. J., Stebel, K., Steinbrecht, W., Strawbridge, K. B., Stübi, R., Swart, D. P. J., Taha,
 1076 G., Tarasick, D. W., Thompson, A. M., Urban, J., van Gijssel, J. A. E., Van Malderen, R.,
 1077 von der Gathen, P., Walker, K. A., Wolfram, E., and Zawodny, J. M.: Ground-based
 1078 assessment of the bias and long-term stability of 14 limb and occultation ozone profile
 1079 data records, *Atmos. Meas. Tech.*, 9, 2497–2534, [https://doi.org/10.5194/amt-9-2497-](https://doi.org/10.5194/amt-9-2497-2016)
 1080 2016, 2016.
- 1081 Jiang, Y. B., Froidevaux, L., Lambert, A., Livesey, N. J., Read, W. G., Waters, J. W., Bojkov,
 1082 B., Leblanc, T., McDermid, I. S., Godin-Beekmann, S., Filipiak, M. J., Harwood, R. S.,
 1083 Fuller, R. A., Daffer, W. H., Drouin, B. J., Cofield, R. E., Cuddy, D. T., Jarnot, R. F.,
 1084 Knosp, B. W., Perun, V. S., Schwartz, M. J., Snyder, W. V., Stek, P. C., Thurstans, R. P.,
 1085 Wagner, P. A., Allaart, M., Andersen, S. B., Bodeker, G., Calpini, B., Claude, H.,
 1086 Coetsee, G., Davies, J., De Backer, H., Dier, H., Fujiwara, M., Johnson, B., Kelder, H.,
 1087 Leme, N. P., König-Langlo, G., Kyro, E., Laneve, G., Fook, L. S., Merrill, J., Morris, G.,
 1088 Newchurch, M., Oltmans, S., Parrondos, M. C., Posny, F., Schmidlin, F., Skrivankova,
 1089 P., Stubi, R., Tarasick, D., Thompson, A., Thouret, V., Viatte, P., Vömel, H., von Der
 1090 Gathen, P., Yela, M., and Zablocki, G.: Validation of Aura Microwave Limb Sounder
 1091 Ozone by ozonesonde and lidar measurements, *J. Geophys. Res.*, 112, D24S34,
 1092 doi:10.1029/2007JD008776, 2007.
- 1093 Johnson, Bryan J.; Cullis, Patrick D.; and NOAA ESRL (2018): Earth System Research
 1094 Laboratory Ozone Water Vapor Group Ozonesonde Measurements, Version 1. NOAA
 1095 National Centers for Environmental Information. doi:10.7289/V5CC0XZ1 [assess in May
 1096 2019]
- 1097 Kar, J., McElroy, C. T., Drummond, J. R., Zou, J., Nichitiu, F., Walker, K. A., Randall, C. E.,
 1098 Nowlan, C. R., Dufour, D. G., Boone, C. D., Bernath, P. F., Treppe, C. R., Thomason, L.
 1099 W., and McLinden, C.: Initial comparison of Ozone and NO₂ profiles from ACE-
 1100 MAESTRO with Balloon and Satellite Data, *J. Geophys. Res.*, 112, D16301,
 1101 doi:10.1029/2006JD008242, 2007
- 1102 Keckhut, P., McDermid, S., Swart, D., McGee, T., Godin Beekmann, S., Adriani, A., Barnes, J.,
 1103 Baray, J.-L., Bencherif, H., Claude, H., di Sarra, A., Fiocco, G., Hansen, G.,
 1104 Hauchecorne, A., Leblanc, T., Lee, C., Pal, S., Megie, G., Nakane, H., Neuber, R.,
 1105 Steinbrecht, W., and Thayer, J.: Review of ozone and temperature lidar validations
 1106 performed within the framework of the Network for the Detection of Stratospheric
 1107 Change, *J. Environ. Monit.*, 6, 721–733, doi:10.1039/b404256e, 2004.
- 1108 Kramarova, N. A., Nash, E. R., Newman, P. A., Bhartia, P. K., McPeters, R. D., Rault, D. F.,
 1109 Seftor, C. J., Xu, P. Q., and Labow, G. J.: Measuring the Antarctic ozone hole with the
 1110 new Ozone Mapping and Profiler Suite (OMPS), *Atmos. Chem. Phys.*, 14, 2353–2361,
 1111 <https://doi.org/10.5194/acp-14-2353-2014>, 2014.
- 1112 Kramarova, N. A., Bhartia, P. K., Jaross, G., Moy, L., Xu, P., Chen, Z., DeLand, M., Froidevaux,
 1113 L., Livesey, N., Degenstein, D., Bourassa, A., Walker, K. A., and Sheese, P.: Validation
 1114 of ozone profile retrievals derived from the OMPS LP version 2.5 algorithm against
 1115 correlative satellite measurements, *Atmos. Meas. Tech.*, 11, 2837–2861,
 1116 <https://doi.org/10.5194/amt-11-2837-2018>, 2018.

- 1117 Kyrölä, E., Laine, M., Sofieva, V., Tamminen, J., Päivärinta, S.-M., Tukiainen, S., Zawodny, J.,
 1118 and Thomason, L.: Combined SAGE II–GOMOS ozone profile data set for 1984–2011
 1119 and trend analysis of the vertical distribution of ozone, *Atmos. Chem. Phys.*, 13, 10645–
 1120 10658, doi:10.5194/acp-13-10645-2013, 2013.
- 1121 Livesey, N. J., W. V. Snyder, W. G. Read, and P. A. Wagner (2006), Retrieval algorithms for the
 1122 EOS Microwave Limb Sounder (MLS), *IEEE Trans. Geosci. Remote Sens.*, 44(5), 1144–
 1123 1155.
- 1124 Livesey N. J., M. J. Filipiak, L. Froidevaux, W. G. Read, A. Lambert, M. L. Santee, J. H.
 1125 Jiang, H. C. Pumphrey, J. W. Waters, R. E. Cofield, D. T. Cuddy, W. H. Daffer, B. J.
 1126 Drouin, R. A. Fuller, R. F. Jarnot, Y. B. Jiang, B. W. Knosp, Q. B. Li, V. S. Perun, M. J.
 1127 Schwartz, W. V. Snyder, P. C. Stek, R. P. Thurstans, P. A. Wagner, M. Avery, E. V.
 1128 Browell, J.-P. Cammas, L. E. Christensen, G. S. Diskin, R.-S. Gao, H.-J. Jost, M.
 1129 Loewenstein, J. D. Lopez, P. Nedelec, G. B. Osterman, G. W. Sachse, C. R. Webster,
 1130 Validation of Aura Microwave Limb Sounder O₃ and CO observations in the upper
 1131 troposphere and lower stratosphere, *J. Geophys. Res.*,
 1132 113,D15S02,doi:10.1029/2007JD008805, 2008.
- 1133 Livesey, Nathaniel J, William G. Read, Paul A. Wagner, Lucien Froidevaux, Alyn Lambert,
 1134 Gloria L. Manney, Luis F. Millán Valle, Hugh C. Pumphrey, Michelle L. Santee, Michael
 1135 J. Schwartz, Shuhui Wang, Ryan A. Fuller, Robert F. Jarnot, Brian W. Knosp, Elmain
 1136 Martinez, Richard R. Lay, Earth Observing System (EOS) Aura Microwave Limb
 1137 Sounder (MLS) Version 4.2x Level 2 data quality and description document, JPL D-
 1138 33509 Rev.D 2018.
- 1139 Llewellyn, E. J., Lloyd, N. D., Degenstein, D. A., Gattinger, R. L., Petelina, S. V, Bourassa, A.
 1140 E., Wiensz, J. T., Ivanov, E. V, Mcdade, I. C., Solheim, B. H., Mcconnell, J. C., Haley,
 1141 C. S., Von Savigny, C., Sioris, C. E., Mclinden, C. A., Griffioen, E., Kaminski, J., Evans,
 1142 W. F. J., Puckrin, E., Strong, K., Wehrle, V., Hum, R. H., Kendall, D. J. W., Matsushita,
 1143 J., Murtagh, D. P., Brohede, S., Stegman, J., Witt, G., Barnes, G., Payne, W. F., Piché, L.,
 1144 Smith, K., Warshaw, G., Deslauniers, D., Marchand, P., Richardson, E. H., King, R. A.,
 1145 Wevers, I., McCreath, W., Kyrölä, E., Oikarinen, L., Leppelmeier, G. W., Auvinen, H.,
 1146 Mégie, G., Hauchecorne, A., Lefèvre, F., De La Nöe, J., Ricaud, P., Frisk, U., Sjoberg,
 1147 F., Von Schéele, F., and Nordh, L.: The OSIRIS instrument on the Odin spacecraft, *Can.*
 1148 *J. Phys.*, 82, 411–422, doi:10.1139/P04-005, 2004.
- 1149 Mauldin, L. E., Zaun, N. H., McCormick, M. P., Guy, J. H., and Vaughn, W. R.: Stratospheric
 1150 Aerosol and Gas Experiment II Instrument: A Functional Description, *Opt. Eng.*, 24,
 1151 307–312, doi:10.1117/ 12.7973473, 1985.
- 1152 Mégie, G., G. Ancellet, and J. Pelon, Lidar measurements of ozone vertical profiles, *Appl. Opt.*,
 1153 24, 3454-3453, 1985
- 1154 McCormick, M. P., J. M. Zawodny, W. P. Chu, J. W. Baer, J. Guy, and A. Ray, Stratospheric
 1155 Aerosol and Gas Experiment III (SAGE III), *SPIE International Symposium for Optical*
 1156 *Engineering* - Orlando, FL, 1993
- 1157 McLinden, C. A., Bourassa, A. E., Brohede, S., Cooper, M., Degenstein, D. A., Evans, W. J. F.,
 1158 Gattinger, R. L., Haley, C. S., Llewellyn, E. J., Lloyd, N. D., Loewen, P., Martin, R. V.,
 1159 McConnell, J. C., McDade, I. C., Murtagh, D., Rieger, L., von Savigny, C., Sheese, P. E.,

- 1160 Sioris, C. E., Solheim, B. and Strong, K.: OSIRIS: A decade of scattered light, *B. Am.*
 1161 *Meteorol. Soc.*, 93, 1845–1863, doi:10.1175/BAMS-D-11-00135.1, 2012.
- 1162 McPeters R. D., Janz, S. J., Hilsenrath, E., and Brown, T. L.: The retrieval of O3 profiles from
 1163 limb scatter measurements: Results from the Shuttle Ozone Limb Sounding Experiment,
 1164 *Geoph. Res. Lett.*, 27, 2597–2600, 2000.
- 1165 Nair, P. J., Godin-Beekmann, S., Froidevaux, L., Flynn, L. E., Zawodny, J. M., Russell III, J. M.,
 1166 Pazmiño, A., Ancellet, G., Steinbrecht, W., Claude, H., Leblanc, T., McDermid, S., van
 1167 Gijssels, J. A. E., Johnson, B., Thomas, A., Hubert, D., Lambert, J.-C., Nakane, H., and
 1168 Swart, D. P. J.: Relative drifts and stability of satellite and ground-based stratospheric
 1169 ozone profiles at NDACC lidar stations, *Atmos. Meas. Tech.*, 5, 1301–1318,
 1170 doi:10.5194/amt-5-1301-2012, 2012.
- 1171 NIMA Technical Report TR8350.2: Department of Defense World Geodetic System 1984, Its
 1172 Definition and Relationships With Local Geodetic Systems, 3rd Edition, 4 July 1997.
- 1173 Parrish, A., Boyd, I. S., Nedoluha, G. E., Bhartia, P. K., Frith, S. M., Kramarova, N. A., Connor, B. J.,
 1174 Bodeker, G. E., Froidevaux, L., Shiotani, M., and Sakazaki, T.: Diurnal variations of
 1175 stratospheric ozone measured by ground-based microwave remote sensing at the Mauna
 1176 Loa NDACC site: measurement validation and GEOSCCM model comparison, *Atmos.*
 1177 *Chem. Phys.*, 14, 7255–7272, <https://doi.org/10.5194/acp-14-7255-2014>, 2014.
- 1178 Pitts, M. C., and L. W. Thomason (2003), SAGE III temperature and pressure retrievals: Initial
 1179 results, *Proc. SPIE Int. Soc. Opt. Eng.*, 482, 62–70.
- 1180 Rault, D. F. (2005), Ozone profile retrieval from Stratospheric Aerosol and Gas Experiment
 1181 (SAGE III) limb scatter measurements, *J. Geophys. Res.*, 110, D09309,
 1182 doi:10.1029/2004JD004970
- 1183 Rault, D. F. and Loughman, R. P.: The OMPS Limb Profiler Environmental Data Record
 1184 Algorithm Theoretical Basis Document and Expected Performance, *IEEE T. Geosci.*
 1185 *Remote Sens.*, 51, 2505–2527, <https://doi.org/10.1109/TGRS.2012.2213093>, 2013.
- 1186 Rodgers, C. D. (2000), *Inverse Methods for Atmospheric Science, Theory and Practice*, 238 pp.,
 1187 World Sci., Hackensack, N.J.
- 1188 Roth, C. Z., Degenstein, D. A., Bourassa, A. E., and Llewellyn, E. J.: The retrieval of vertical
 1189 profiles of the ozone number density using Chappuis band absorption information and a
 1190 multiplicative algebraic reconstruction technique, *Can. J. Phys.*, 85, 1225–1243,
 1191 doi:10.1139/P07-130, 2007.
- 1192 SAGE III ATBD: SAGE III Algorithm Theoretical Basis Document: Solar and Lunar Algorithm,
 1193 Earth Observing System Project Science Office web site online available at:
 1194 <https://eosps.gsfc.nasa.gov/sites/default/files/atbd/atbd-sage-solar-lunar.pdf>, 2002
- 1195 Sakazaki, T., Fujiwara, M., Mitsuda, C., Imai, K., Manago, N., Naito, Y., Nakamura, T.,
 1196 Akiyoshi, H., Kinnison, D., Sano, T., Suzuki, M., and Shiotani, M.: Diurnal ozone
 1197 variations in the stratosphere revealed in observations from the Superconducting
 1198 Submillimeter-Wave Limb-Emission Sounder (SMILES) on board the International
 1199 Space Station (ISS), *J. Geophys. Res. Atmos.*, 118, 2991–3006, doi:10.1002/jgrd.50220,
 1200 2013.

- 1201 Sakazaki, T., Shiotani, M., Suzuki, M., Kinnison, D., Zawodny, J. M., McHugh, M., and Walker,
 1202 K. A.: Sunset–sunrise difference in solar occultation ozone measurements (SAGE II,
 1203 HALOE, and ACE–FTS) and its relationship to tidal vertical winds, *Atmos. Chem. Phys.*,
 1204 15, 829–843, <https://doi.org/10.5194/acp-15-829-2015>, 2015
- 1205 Sheese, P. E., Boone, C. D., and Walker, K. A.: Detecting physically unrealistic outliers in ACE-
 1206 FTS atmospheric measurements, *Atmos. Meas. Tech.*, 8, 741–750,
 1207 <https://doi.org/10.5194/amt-8741-2015>, 2015.
- 1208 Smit, H. G. J. and the Panel for the Assessment of Standard Operating Procedures for
 1209 Ozonesondes (ASOPOS): Quality Assurance and Quality Control for Ozone
 1210 Measurements in GAW, WMO Global Atmosphere Watch report No. 201, World
 1211 Meteorological Organization, available at:
 1212 https://library.wmo.int/pmb_ged/gaw_201_en.pdf (last access: 22 July 2019), 2014.
- 1213 Sofieva, V. F., Tamminen, J., Kyrölä, E., Laeng, A., von Clarmann, T., Dalaudier, F.,
 1214 Hauchecorne, A., Bertaux, J.-L., Barrot, G., Blanot, L., Fussen, D., and Vanhellemont, F.:
 1215 Validation of GOMOS ozone precision estimates in the stratosphere, *Atmos. Meas. Tech.*,
 1216 7, 2147–2158, <https://doi.org/10.5194/amt-7-2147-2014>, 2014.
- 1217 Sheese, P. E., Walker, K. A., Boone, C. D., Bernath, P. F., Froidevaux, L., Funke, B., and von
 1218 Clarmann, T.: ACE-FTS ozone, water vapour, nitrous oxide, nitric acid, and carbon
 1219 monoxide profile comparisons with MIPAS and MLS, *J. Quant. Spectrosc. Ra.*, 186, 63–
 1220 80, <https://doi.org/10.1016/j.jqsrt.2016.06.026>, 2017.
- 1221 SPARC/IO3C/GAW, 2019: SPARC/IO3C/GAW Report on Long-term Ozone Trends and
 1222 Uncertainties in the Stratosphere. I. Petropavlovskikh, S. Godin-Beekmann, D. Hubert, R.
 1223 Damadeo, B. Hassler, V. Sofieva (Eds.), SPARC Report No. 9, GAW Report No. 241,
 1224 WCRP-17/2018, doi: 10.17874/f899e57a20b
- 1225 SPARC, 2006: SPARC Assessment of Stratospheric Aerosol Properties (ASAP). L. Thomason
 1226 and Th. Peter (Eds.), SPARC Report No. 4, WCRP-124, WMO/TD – No. 1295
- 1227 Thomason, L. W., Moore, J. R., Pitts, M. C., Zawodny, J. M., and Chiou, E. W.: An evaluation
 1228 of the SAGE III version 4 aerosol extinction coefficient and water vapor data products,
 1229 *Atmos. Chem. Phys.*, 10, 2159–2173, <https://doi.org/10.5194/acp-10-2159-2010>, 2010
- 1230 Thompson, A. M., J. C. Witte, C., Sterling, A., Jordan, B. J., Johnson, S. J. Oltmans, ... Thiongo,
 1231 K. (2017). First reprocessing of Southern Hemisphere Additional Ozonesondes
 1232 (SHADOZ) ozone profiles (1998–2016): 2. Comparisons with satellites and ground-based
 1233 instruments. *Journal of Geophysical Research: Atmospheres*, 122, 13,000–13,025.
 1234 <https://doi.org/10.1002/2017JD 027406>.
- 1235 von Clarmann, T.: Validation of remotely sensed profiles of atmospheric state variables:
 1236 strategies and terminology, *Atmos. Chem. Phys.*, 6, 4311–4320,
 1237 <https://doi.org/10.5194/acp-6-4311-2006>, 2006.
- 1238 Wang, H. J., D. M. Cunnold, and X. Bao, A critical analysis of SAGE ozone trends, *J. Geophys.*
 1239 *Res.*, 101, 12,495–12,514, 1996.
- 1240 Wang, H. J., D. M. Cunnold, L. W. Thomason, J. M. Zawodny, and G. E. Bodeker, Assessment
 1241 of SAGE version 6.1 ozone data quality, *J. Geophys. Res.*, 107(D23), 4691,
 1242 doi:10.1029/2002JD002418, 2002.

- 1243 Wang, H.-J., Cunnold, D. M., Trepte, C., Thomason, L. W., Zawodny J. M.: SAGE III solar
1244 ozone measurements: Initial results, *Geophys. Res. Lett.*, 33, L03805,
1245 doi:10.1029/2005GL025099, 2006.
- 1246 Waters, J. W., Froidevaux, L., Harwood, R. S., Jarnot, R. F., Pickett, H. M., Read, W. G., Siegel,
1247 P. H., Cofield, R. E., Filipiak, M. J., Flower, D. A., Holden, J. R., Lau, G. K., Livesey, N.
1248 J., Manney, G. L., Pumphrey, H. C., Santee, M. L., Wu, D. L., Cuddy, D. T., Lay, R. R.,
1249 Loo, M. S., Perun, V. S., Schwartz, M. J., Stek, P. C., Thurstans, R. P., Boyles, M. A.,
1250 Chandra, K. M., Chavez, M. C., Chen, G., Chudasama, B. V, Dodge, R., Fuller, R. A.,
1251 Girard, M. A., Jiang, J. H., Jiang, Y., Knosp, B. W., Labelle, R. C., Lam, J. C., Lee, K.
1252 A., Miller, D., Oswald, J. E., Patel, N. C., Pukala, D. M., Quintero, O., Scaff, D. M.,
1253 Snyder, W. Van, Tope, M. C., Wagner, P. A., and Walch, M. J.: The Earth Observing
1254 System Microwave Limb Sounder (EOS MLS) on the Aura Satellite, *IEEE T. Geosci.*
1255 *Remote*, 44, 1075–1092, 2006.
- 1256 Witte, J.C., A. M. Thompson, H. G. J. Smit, M. Fujiwara, F. Posny, Gert J. R. Coetzee, E. T.
1257 Northam, B. J. Johnson, C, W, Sterling, M. Mohamad, S. Ogino, A. Jordan, and F. R. da
1258 Silva (2017), First reprocessing of Southern Hemisphere ADDitional OZonesondes
1259 (SHADOZ) profile records (1998-2015): 1. Methodology and evaluation, *J. Geophys.*
1260 *Res. Atmos.*, 122, 6611-6636. <https://doi.org/10.1002/2016JD026403>.
- 1261 WMO (World Meteorological Organization), Scientific Assessment of Ozone Depletion: 2018,
1262 Global Ozone Research and Monitoring Project–Report No. 58, 588 pp., Geneva,
1263 Switzerland, 2018.
- 1264 Zawada DJ, Dueck SR, Rieger LA, Bourassa AE, Lloyd ND, Degenstein DA, High-resolution
1265 and Monte Carlo additions to the SASKTRAN radiative transfer model, *Atmos. Meas.*
1266 *Tech.*, 8, 2609-2623, 2015
- 1267